performed using Moloney murine leukemia virus reverse transcriptase, random hexamers, and oligoT (all from Promega) according to the manufacturer's instructions. Glyceraldehyde-3-phosphate dehydrogenase (GAPDH) was used as a housekeeping gene. Primer sequences (5′ → 3′) were as follows: NANOG (AAACCATGGATTTATTCCTAA and AGGAAGGATTCAGCCAGT), REX1 (TTCGTGTGTCCCTTTCAA and TTGTTCATTCTTGTTCGT), TDGF1 (GAGATGACAGCATTTGGC and GGCAGCAGGTTCTGTTTA), SeV (AGACCCTAAGAGGACGAAGACAGA and ACTCCCATGGCGTA ACTCCATAG), and GAPDH (CATCCATGACAACTTTGG and GCTTCC CGTTCAGCTC).

Analysis of T-Cell Receptor β-Chain Rearrangements in iPSC Clones

Genomic DNA of iPSC clones was isolated using a Puregene kit (Qiagen) according to the manufacturer's instructions. Before the experiments, the quality of all DNA samples was tested in the polymerase chain reaction (PCR) with a control size ladder mix provided by the TCRB Gene Clonality assay kit (Invivoscribe, San Diego, CA, http://www.invivoscribe.com). T-cell clonal DNA (IVS0004) was used as a positive control for all specific multiplex PCRs, performed according to the kit instructions (Invivoscribe). Human ES cell line H9 was used as a negative control. T-cell receptor (TCR)-β PCR products were detected in 2% agarose gel, and fragment analysis was performed in the sequencing unit of the FIMM Technology Centre by capillary electrophoresis using ABI3730 DNA analyzer. Peak Scanner software (Applied Biosystems, Foster City, CA, http://www.appliedbiosystems.com) was used for fragment size analysis.

RESULTS

Production of PBMC-Derived iPSCs Using the 4V Method

Generation of iPSC from activated T-cells using Sendai virus (SeV) each carrying individually one of the four Yamanaka factors (OCT4, SOX2, KLF4, and c-MYC) has previously been reported [9, 10]. We therefore reprogrammed both activated and nonactivated PBMCs (n = 3 donors) using commercially available Cytotune-iPS reprogramming kit, referred to here as the 4V method. The first iPSC-like colonies appeared at day 15. By day 21, iPSC colonies with morphology similar to embryonic stem cells (ESCs) were picked and expanded (Fig. 1). The mean reprogramming efficiency was determined to be 0.005% (n = 3, SD = 0.001) measured as the ratio of produced iPSC colonies to the starting PBMC cell number (supplemental online Fig. 1). The optimal conditions for PBMC reprogramming were determined to be 3×10^5 cells infected with MOI 3.

All iPSC clones (n = 8) stained positive for stem cell markers OCT4, SSEA4, and TRA-1-60 as detected by immunofluorescence and expressed NANOG, TDGF1, and REX1 as detected by RT-PCR (Fig. 1). Notably, iPSC colonies were only detected from the preactivated PBMCs, and no colonies appeared from the nonactivated PBMCs directly infected with the 4V method, indicating that activated T cells are the most probable target of SeV infection.

Reprogramming of PBMCs by Tetracistronic SeVdp

The use of polycistronic SeV enables balanced expression of all transgenes, which increases reprogramming efficiency [7, 20]. Therefore, we next reprogrammed PBMCs using replication-defective and persistent SeV (SeVdp), which accommodates all

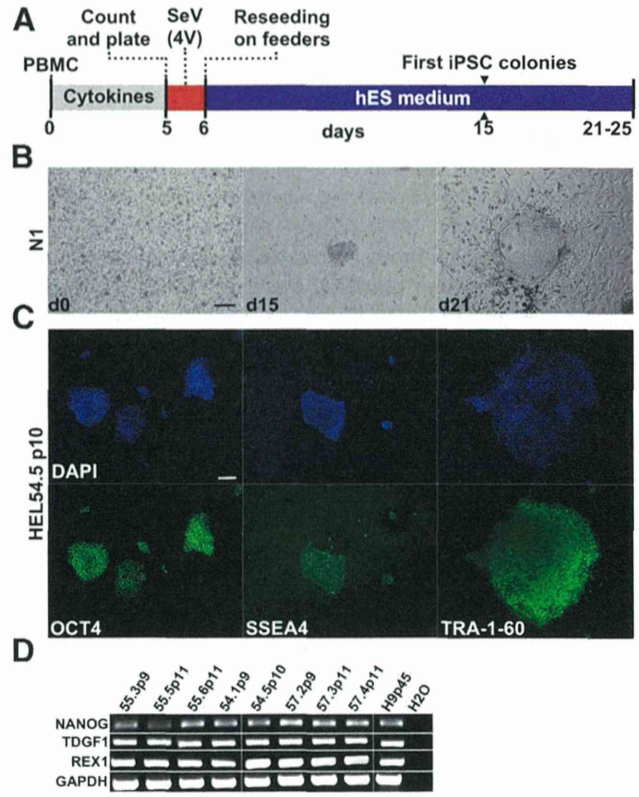

Figure 1. Reprogramming using the 4V method. **(A):** Schematic presentation of reprogramming using Cytotune iPS reprogramming kit (referred to as the 4V method in the text) producing iPSCs only from the activated PBMCs. **(B):** Morphology of reprogrammed PBMCs at days 0, 15, and 21 from one representative donor (N1). **(C):** Expression of stem cell markers from one representative iPSC line (HEL54.5): OCT4 (green), SSE4 (green), and TRA-1-60 (green) and nuclear staining with DAPI (blue). **(D):** Reverse transcription-polymerase chain reaction from generated iPSC lines, stem cell markers: NANOG, TDGF1, REX1, and housekeeping gene GAPDH. Scale bars = 200 μm. Abbreviations: d, day; DAPI, 4′,6-diamidino-2-phenylindole; GAPDH, glyceraldehyde-3-phosphate dehydrogenase; hES, human embryonic stem cell; iPSC, induced pluripotent stem cell; PBMC, peripheral blood mononuclear cell; SeV (4V), Sendai virus (Cytotune).

four Yamanaka factors in a single vector [7]. PBMCs from three donors were infected with or without preceding cell activation and seeded on feeder cells. The first iPSC-like colonies appeared on plates originating from nonactivated PBMCs already at day 6, and by day 16, the colonies were large enough for passaging (supplemental online Fig. 1). Mean reprogramming efficiency was found to be 0.014% $\pm$ 0.006% (mean $\pm$ SD of two separate experiments with three different donors), which is higher compared with the 4V method (supplemental online Fig. 1D). A total of nine iPSC clones were further characterized. All iPSC lines expressed stem cell markers as determined by immunofluorescence and RT-PCR and were able to differentiate into cells derivative of all three germ layers by spontaneous differentiation (data not shown).

Generation of iPSCs Directly From PBMCs in Feeder-Free Conditions

Encouraged by the efficient reprogramming of PBMCs without cell activation on feeders, we performed SeVdp-mediated inductions from three different donors in feeder-free conditions (Fig. 2A). The first iPSC-like colonies were observed firmly attached

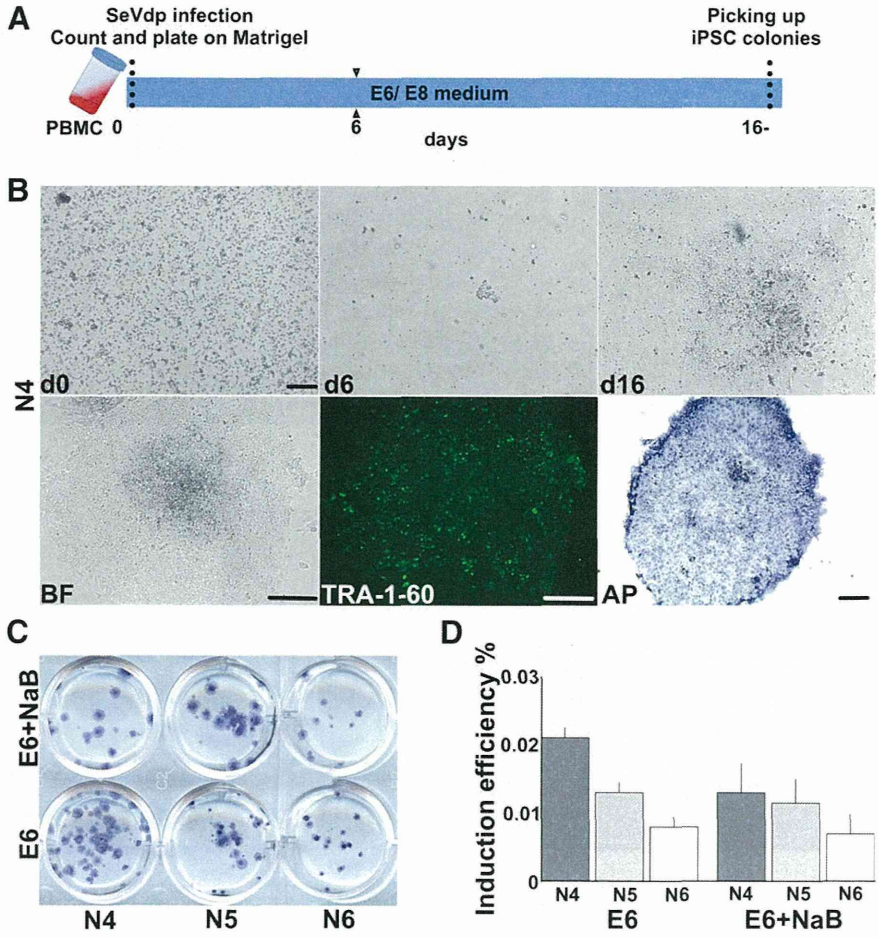

Figure 2. Reprogramming of PBMCs in a feeder-free conditions by SeVdp. **(A):** Schematic representation of PBMC reprogramming using SeVdp, which produces iPSCs from the intact PBMCs. **(B):** Morphology of reprogrammed PBMCs at days 0, 6, and 16. BF, TRA-1-60 (green), and AP staining (blue) of bona fide iPSCs at day 16, shown from one representative induction (N4). **(C, D):** Reprogramming efficiency of PBMCs of three donors (N4, N5, and N6) with and without NaB was determined using AP staining. Induction efficiency is shown as percentages (*y*-axis). Scale bars = 200 μm. Abbreviations: AP, alkaline phosphatase; BF, bright field; d, day; iPSC, induced pluripotent stem cell; NaB, sodium butyrate; PBMC, peripheral blood mononuclear cell; SeVdp, tetracistronic Sendai virus.

to the culture plates already at day 6 after induction (Fig. 2B). At this time point, cells were rounded with clear cell-to-cell boundaries. By day 16, cells adhered to each other and formed large ESC-like colonies with distinct borders containing tightly packed cells with high nucleus/cytoplasm ratios and prominent nucleoli. The colonies stained positively for alkaline phosphatase and were visualized by live immunostaining using an antibody against TRA-1-60 (Fig. 2B). Mean reprogramming efficiency was determined to be 0.011% $\pm$ 0.006% (n = 6), being similar to SeVdp-mediated induction on feeder cells.

It has been previously reported that addition of NaB to the reprogramming cocktail improves the retrovirus-mediated reprogramming efficiency of fibroblasts and myoblasts [12, 21]. Therefore, we tested whether the addition of NaB could further enhance the formation of iPSCs in feeder-free conditions. However, the addition of NaB to the reprogramming cocktail did not increase the mean reprogramming efficiency, which was found to be 0.01% $\pm$ 0.004% (n = 6) (Fig. 2C, 2D).

Six iPSC clones generated from three different donors were picked at day 16 and further propagated in feeder-free conditions for at least 10 passages. All iPSC lines expressed stem cell markers TRA-1-60, SSEA4, and OCT4 as determined by immunocytochemistry (Fig. 3A). Stem cell markers NANOG, TDGF1, and REX1 were also expressed in all iPSC lines as determined by RT-PCR (Fig. 3B). In addition, all iPSC lines were able to form EBs and spontaneously differentiate into derivatives of all three germline lineages analyzed by neuroectodermal (TUJ1), endodermal (AFP), and mesodermal (VIMENTIN) marker expression (Fig. 3C), indicating their pluripotent nature. The pluripotent nature of the produced iPSC lines (n = 5) was further confirmed using PluriTest [22] (Fig. 3D).

Clearance of SeV Vectors and Origin of iPSC Lines

Ideally, the produced iPSC lines are transgene-free. Two of eight iPSC clones (25%) generated using 4V were still found to be positive for SeV episome. On the contrary, all iPSC clones generated by SeVdp (n = 15) were completely clear of viral sequences by passage 10 (supplemental online Fig. 1E, 1F). In comparison, we also analyzed the clearance of viral sequences from fibroblast-derived iPSC clones (n = 59 iPSC lines generated from 23 donors) reprogrammed using the 4V method. Similarly to the PBMC-derived iPSCs, SeV episomes were still found to be present in 16 of 59 (27%) of the fibroblast-derived iPSC lines by passage 14

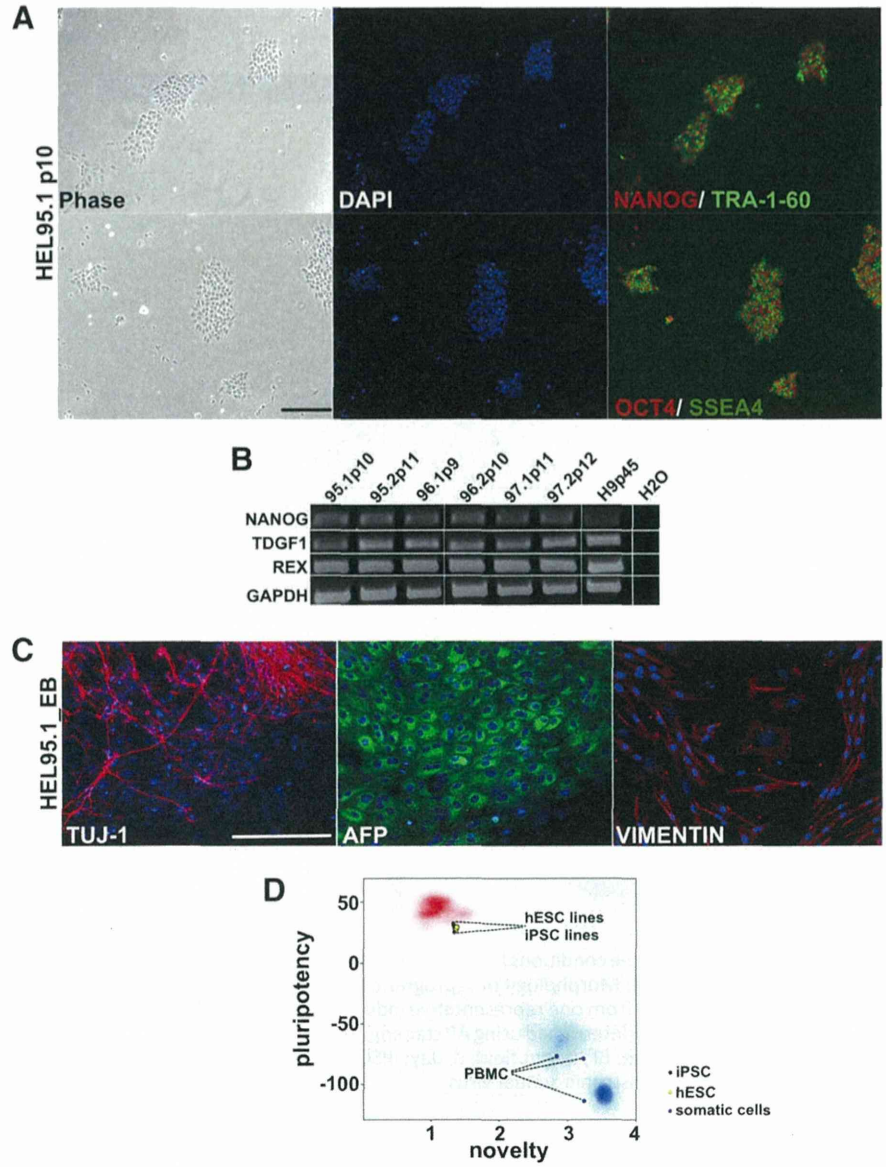

Figure 3. Characterization of iPSC lines generated from PBMCs in feeder-free conditions. **(A):** Morphology of generated iPSC lines (phase), nuclear staining DAPI (blue), stem cell markers: NANOG (red), OCT4 (red), TRA-1-60 (green), and SSEA4 (green). **(B):** Reverse transcription-polymerase chain reaction of PBMC-derived iPSC lines. The stem cell markers were NANOG, TDGF1, and REX1, and housekeeping gene GAPDH. **(C):** Spontaneous differentiation of PBMC-derived iPSCs. Shown are immunostainings of neuronal TUJ1 (red), endodermal AFP (green), and mesodermal VIMENTIN (red) lineage markers, and nuclear staining DAPI (blue); data shown are from one representative iPSC line (HEL95.1). **(D):** Pluripotent transcriptional profile measured in PluriTest. iPSC lines (n = 5) and hES cell lines (n = 2) qualified as a pluripotent as determined by the pluripotency and novelty scores. Donor PBMCs (n = 3) are plotted in the previously referenced somatic cells (blue cloud). Scale bar = 200 μm. Abbreviations: AFP, α-fetoprotein; DAPI, 4′,6-diamidino-2-phenylindole; GAPDH, glyceraldehyde-3-phosphate dehydrogenase; hES, human embryonic stem cell; iPSC, induced pluripotent stem cell; PBMC, peripheral blood mononuclear cell.

(supplemental online Fig. 1F). Further passaging of fibroblast-derived iPSCs did not completely clear the SeV episome, because 7 of 16 of iPSC lines (44%) remained positive for SeV sequences also at later passages (p14–21).

Origin of iPSC Lines

The fact that the two SeV systems infect activated and nonactivated PBMCs with different efficiency suggests that the iPSCs originate from different cell types present in PBMCs. Reprogramming with the 4V method was completely dependent on preceding T-cell activation, suggesting that the produced iPSC clones originate from T lymphocytes. T-cell origin can be analyzed by detecting the specific TCR rearrangements naturally occurring during T-cell development. We performed a multiplex PCR of the genomic TCR-β region of the iPSC lines produced with 4V (n = 8 clones) and with SeVdp (n = 15 clones) and analyzed the results by the gel electrophoresis (supplemental online Fig. 2) and by capillary electrophoresis using ABI3730 DNA analyzer (Fig. 4). The majority of the iPSC clones (7 of 8) produced by the 4V method were positive for TCR-β rearrangements indicating their T-cell origin, whereas none of the SeVdp-induced clones (n = 15) showed TCR-β rearrangements (Fig. 4).

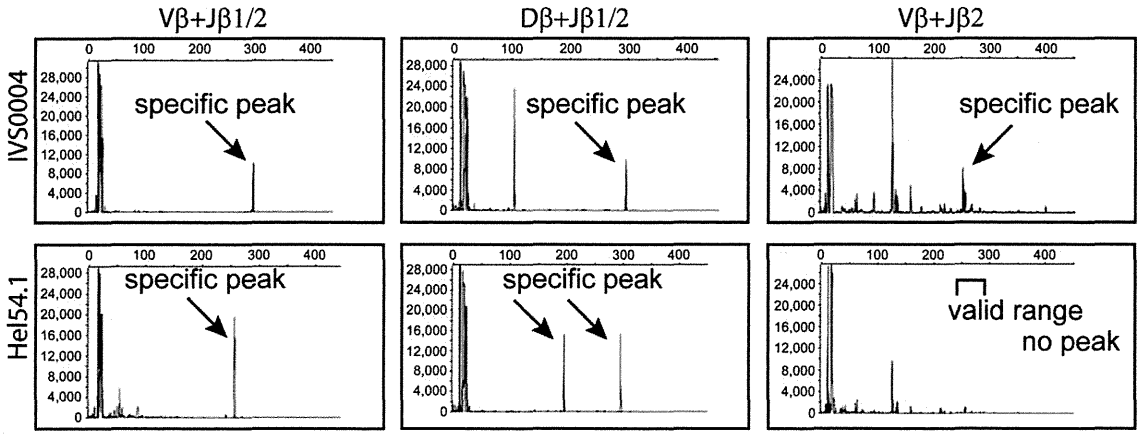

Sample	Cell type	Induction method	Vβ+Jβ 1/2 (240-285)	Dβ+Jβ 1/2 (170-210, 285-325)	Vβ+Jβ2 (240-285)	T-cell origin
Hel54.1	iPS	4V	257	195, 296	---	yes
Hel54.5	iPS	4V	---	181, 304	266	yes
Hel55.2	iPS	4V	---	---	---	no
Hel55.5	iPS	4V	---	308	267	yes
Hel55.6	iPS	4V	261	307	---	yes
Hel57.2	iPS	4V	248	297, 307	---	yes
Hel57.3	iPS	4V	248	298	---	yes
Hel57.4	iPS	4V	267	---	---	yes
Hel95.1	iPS	SeVdp	---	---	---	no
Hel95.2	iPS	SeVdp	---	---	---	no
Hel95.3	iPS	SeVdp	---	---	---	no
Hel96.1	iPS	SeVdp	---	---	---	no
Hel96.2	iPS	SeVdp	---	---	---	no
Hel97.3	iPS	SeVdp	---	---	---	no
Hel97.4	iPS	SeVdp	---	---	---	no
Hel97.1	iPS	SeVdp	---	---	---	no
Hel97.2	iPS	SeVdp	---	---	---	no
Hel51.2	iPS	SeVdp	---	---	---	no
Hel51.3	iPS	SeVdp	---	---	---	no
Hel52.2	iPS	SeVdp	---	---	---	no
Hel52.3	iPS	SeVdp	---	---	---	no
Hel64.1	iPS	SeVdp	---	---	---	no
Hel64.3	iPS	SeVdp	---	---	---	no
IVS0004	T-cell clonal control	---	295	295	253	yes
H9	hES	---	---	---	---	no

Figure 4. Origin of iPSCs. Multiplex polymerase chain reaction fragment size analysis of T-cell receptor β region was performed by capillary electrophoresis using ABI3730 DNA analyzer. Specific peak profiles are shown for positive clonal T-cell control (IVS0004) and for one representative iPSC line (HEL54.1) produced by the 4V method. Fragment sizes for all iPSC clones are indicated in the table. DNA from hES cells (H9) was used as a negative control for the experiments. Abbreviations: 4V, Sendai virus (Cytotune); hES, human embryonic stem cell; iPSC, induced pluripotent stem cell; SeVdp, tetracistronic Sendai virus.

Discussion

Retroviral vectors have mostly been used in the delivery of inducing transgenes into somatic cells during reprogramming. However, retro- and lentivirus vectors are integrated into the parental cell genome. Integration may result in undesirable changes such as malignancy in the produced iPSC lines [23] or reactivation of transgenes during iPSC differentiation [24]. In addition, there is a minimal risk of production of replication- competent HIV by homologous recombination events if lentivirus vectors are used for the induction of HIV-positive donor cells [25] that may be present in the large sample cohorts. HIV testing prior to induction is ethically questionable and increases the costs of reprogramming. For these reasons, nonintegrative methods are more suitable for large-scale reprogramming.

Reprogramming of blood cells in a large scale has been problematic because of the inefficient delivery of transgenes into terminally differentiated blood cells. This problem has been bypassed by inducing more immature blood cell precursors or by activating proliferation of different subpopulations present

in PBMCs [8, 10, 11, 13, 14]. Besides raising the costs and time required for iPSC production, stimulation of cell proliferation may result in generation of several iPSC lines from the same parental cell population that may lead to distortion of data obtained from parallel iPSC clones.

One of the clear advantages of using a polycistronic viral vector for transgene delivery is the synchronized expression of all induction factors in the target cells. Reprogramming efficiency of PBMCs using SeVdp was detected to be on average 0.01%, which was considerably higher compared with the efficiency obtained here by the 4V method (0.005%). The power of providing all transgenes in a single virus (SeVdp) compared with the 4V system (Cyto-Tune) has previously been shown in fibroblast reprogramming [7]. The efficiency of SeVdp-mediated reprogramming was lower than what has been reported for the DNA plasmid-based reprogramming of PBMCs (0.06%) [13]. However, the high efficiency of DNA plasmid-mediated induction was achieved by adding the *EBNA1* and inhibition of *TP53* by small hairpin RNA to the reprogramming cocktail, in addition to stimulating cell growth by cytokine activation [13]. Although downregulation of *TP53* is temporal during reprogramming [26, 27], it is possible that transient downregulation of *TP53* is favorable for cells with genomic aberrations, which would otherwise be eliminated during induction, increasing the probability of acquiring iPSC clones with poor genomic quality [28]. High reprogramming efficiency of PBMCs has recently also been obtained with a modified set of DNA plasmids containing a strong spleen focus-forming virus promoter and anti-apoptotic factor *BCL-XL*, making this method also noteworthy for induction of blood cells [15]. However, episomal DNA plasmids have been shown to undergo occasional genomic integration, resulting in laborious screening of the generated iPSC lines [29].

Importantly, iPSC clones generated by the SeVdp method were all clear of exogenic sequences by passage 10, even without active elimination of replicons. Clearance of SeVdp genome is semiautomatic in response to induction of mir302 in generated nascent iPSC colonies. If required, the removal of transgenes can be enhanced by small interfering RNA treatment [7, 30]. Using this method, we were able to produce iPSC clones from low amounts of PBMCs with minimal amount of virus. We were also able to shorten the generation time of iPSC clones to 16 days, which is approximately 1 week less than with the 4V method. The SeVdp induction did not require activation steps of PBMC subpopulations with cytokines, thus reducing the time and the cost of reprogramming. Importantly, PBMCs were also reprogrammed and maintained in feeder-free conditions, which is a prerequisite for any iPSC biobanking strategy.

Mononuclear cells extracted from peripheral blood contain cells from both lymphoid and nonlymphoid origin. Cytokine stimulation can activate the cell fate or growth and direct induction to the specific cell type. As expected, and also previously reported, activation of T cells was a prerequisite for reprogramming with 4V and resulted in iPSC clones carrying specific TCR rearrangements [10]. However, the iPSC lines should represent the genomic DNA of the donor, lacking T- and B-cell-related DNA rearrangements. The SeVdp-mediated method used in this study did not require cytokine treatment, and the iPSC clones were shown to originate from cells other than T-lymphocytes. Target specificity of SeV vectors is restricted primarily by the initial phase of infection, e.g., fusion between virus envelope and cell membrane [31]. As a result, SeV can infect monocytes and CD4(−)/CD8(−) T cells, but not B cells and CD4(+) T cells [31, 32]. Therefore, it is likely that SeVdp-mediated iPSC clones analyzed in this study originate from cells other than T or B cells and therefore do not carry major genetic rearrangements found in TCR and immunoglobulin regions. The fact that SeVdp virus preferred nonlymphoid cells as its target in the intact PBMC pool to the increased number of T cells in the activated PBMC sample suggests that in addition to virus efficiency, different cell sensitivity also contributes to the reprogramming power.

Nonlymphoid cells of PBMCs have previously been targeted by cytokine induction both by DNA plasmids and viral vectors [8, 15]. It was recently shown that iPSCs generated from human finger prick using the 4V system do not contain T-cell-specific genomic rearrangements [33]. However, extensive expansion of PBMCs with cytokines is required prior to infection with SeV carrying the Yamanaka reprogramming factors.

Conclusion

Our study demonstrates that PBMCs can be efficiently reprogrammed without cytokine activation directly from PBMCs in feeder-free conditions in just 16 days. The generated iPSC lines are transgene-free and do not contain genomic rearrangement. Thus, our reprogramming system has potential to advance large-scale reprogramming of PBMCs into iPSCs for biobanking purposes.

Acknowledgments

The SeVdp vector was produced in the National Institute of Advanced Industrial Science and Technology (AIST), and is available upon request (mahito-nakanishi@aist.go.jp). This work was supported by the Academy of Finland (Grant 271884), the Sigrid Jusélius Foundation, and the Research Funds of the Helsinki University Central Hospital. We thank Anne Nyberg, Seija Puomilahti, Jarkko Ustinov, and Eila Korhonen for excellent technical assistance. We also thank Jarno Honkanen (Department of Vaccination and Immune Protection, National Institute for Health and Welfare, Helsinki, Finland) for the protocol for T-cell activation. We thank the participants of the FINRISK 2012 study. K.N. is currently affiliated with the Laboratory of Gene Regulation, Faculty of Medicine, University of Tsukuba, Tsukuba, Ibaraki, Japan.

Author Contributions

R.T. and A.K.: conception and design, collection and/or assembly of data, data analysis and interpretation, manuscript writing, final approval of manuscript; J.W.: collection and/or assembly of data, final approval of manuscript; K.N. and M.O.: conception and design, final approval of manuscript, generation of SeVdp vector; M.N.: conception and design, manuscript writing, final approval of manuscript, generation of SeVdp vector; V.S.: provision of study material or patients, final approval of manuscript; A.J. and T.O.: financial support, final approval of manuscript.

Disclosure of Potential Conflicts of Interest

The authors indicate no potential conflicts of interest.

REFERENCES

1 Takahashi K, Tanabe K, Ohnuki M et al. Induction of pluripotent stem cells from adult human fibroblasts by defined factors. Cell 2007; 131:861–872.

2 Takahashi K, Yamanaka S. Induction of pluripotent stem cells from mouse embryonic and adult fibroblast cultures by defined factors. Cell 2006;126:663–676.

3 Okita K, Nakagawa M, Hyenjong H et al. Generation of mouse induced pluripotent stem cells without viral vectors. Science 2008;322: 949–953.

4 Yu J, Hu K, Smuga-Otto K et al. Human induced pluripotent stem cells free of vector and transgene sequences. Science 2009;324:797–801.

5 Weltner J, Anisimov A, Alitalo K et al. Induced pluripotent stem cell clones reprogrammed via recombinant adeno-associated virus-mediated transduction contain integrated vector sequences. J Virol 2012;86:4463–4467.

6 Fusaki N, Ban H, Nishiyama A et al. Efficient induction of transgene-free human pluripotent stem cells using a vector based on Sendai virus, an RNA virus that does not integrate into the host genome. Proc Jpn Acad Ser B Phys Biol Sci 2009;85:348–362.

7 Nishimura K, Sano M, Ohtaka M et al. Development of defective and persistent Sendai virus vector: A unique gene delivery/ expression system ideal for cell reprogramming. J Biol Chem 2011;286:4760–4771.

8 Loh YH, Hartung O, Li H et al. Reprogramming of T cells from human peripheral blood. Cell Stem Cell 2010;7:15–19.

9 Seki T, Yuasa S, Fukuda K. Generation of induced pluripotent stem cells from a small amount of human peripheral blood using a combination of activated T cells and Sendai virus. Nat Protoc 2012;7:718–728.

10 Seki T, Yuasa S, Oda M et al. Generation of induced pluripotent stem cells from human terminally differentiated circulating T cells. Cell Stem Cell 2010;7:11–14.

11 Staerk J, Dawlaty MM, Gao Q et al. Reprogramming of human peripheral blood cells to induced pluripotent stem cells. Cell Stem Cell 2010;7:20–24.

12 Trokovic R, Weltner J, Manninen T et al. Small molecule inhibitors promote efficient generation of induced pluripotent stem cells from human skeletal myoblasts. Stem Cells Dev 2013;22:114–123.

13 Okita K, Yamakawa T, Matsumura Y et al. An efficient nonviral method to generate integration-free human-induced pluripotent stem cells from cord blood and peripheral blood cells. STEM CELLS 2013;31:458–466.

14 Dowey SN, Huang X, Chou BK et al. Generation of integration-free human induced pluripotent stem cells from postnatal blood mononuclear cells by plasmid vector expression. Nat Protoc 2012;7:2013–2021.

15 Su RJ, Baylink DJ, Neises A et al. Efficient generation of integration-free iPS cells from human adult peripheral blood using BCL-XL together with Yamanaka factors. PLoS One 2013;8:e64496.

16 Ye L, Muench MO, Fusaki N et al. Blood cell-derived induced pluripotent stem cells free of reprogramming factors generated by Sendai viral vectors. STEM CELLS TRANSLATIONAL MEDICINE 2013;2:558–566.

17 Wakao H, Yoshikiyo K, Koshimizu U et al. Expansion of functional human mucosal-associated invariant T cells via reprogramming to pluripotency and redifferentiation. Cell Stem Cell 2013;12:546–558.

18 Nishimura T, Kaneko S, Kawana-Tachikawa A et al. Generation of rejuvenated antigen-specific T cells by reprogramming to pluripotency and redifferentiation. Cell Stem Cell 2013;12:114–126.

19 Vartiainen E, Laatikainen T, Peltonen M et al. Thirty-five-year trends in cardiovascular risk factors in Finland. Int J Epidemiol 2010;39:504–518.

20 Nakanishi M, Otsu M. Development of Sendai virus vectors and their potential applications in gene therapy and regenerative medicine. Curr Gene Ther 2012;12:410–416.

21 Mali P, Chou BK, Yen J et al. Butyrate greatly enhances derivation of human induced pluripotent stem cells by promoting epigenetic remodeling and the expression of pluripotency-associated genes. STEM CELLS 2010;28:713–720.

22 Müller FJ, Schuldt BM, Williams R et al. A bioinformatic assay for pluripotency in human cells. Nat Methods 2011;8:315–317.

23 Okita K, Yamanaka S. Induced pluripotent stem cells: Opportunities and challenges. Philos Trans R Soc Lond B Biol Sci 2011;366: 2198–2207.

24 Toivonen S, Ojala M, Hyysalo A et al. Comparative analysis of targeted differentiation of human induced pluripotent stem cells (hiPSCs) and human embryonic stem cells reveals variability associated with incomplete transgene silencing in retrovirally derived hiPSC lines. STEM CELLS TRANSLATIONAL MEDICINE 2013;2: 83–93.

25 Connolly JB. Lentiviruses in gene therapy clinical research. Gene Ther 2002;9:1730–1734.

26 Kawamura T, Suzuki J, Wang YV et al. Linking the p53 tumour suppressor pathway to somatic cell reprogramming. Nature 2009; 460:1140–1144.

27 Hong H, Takahashi K, Ichisaka T et al. Suppression of induced pluripotent stem cell generation by the p53-p21 pathway. Nature 2009; 460:1132–1135.

28 González F, Georgieva D, Vanoli F et al. Homologous recombination DNA repair genes play a critical role in reprogramming to a pluripotent state. Cell Reports 2013;3:651–660.

29 Okita K, Matsumura Y, Sato Y et al. A more efficient method to generate integration-free human iPS cells. Nat Methods 2011;8:409–412.

30 Kawagoe S, Higuchi T, Otaka M et al. Morphological features of iPS cells generated from Fabry disease skin fibroblasts using Sendai virus vector (SeVdp). Mol Genet Metab 2013;109: 386–389.

31 Watabe A, Yamaguchi T, Kawanishi T et al. Target-cell specificity of fusogenic liposomes: Membrane fusion-mediated macromolecule delivery into human blood mononuclear cells. Biochim Biophys Acta 1999;1416:339–348.

32 Eguchi A, Kondoh T, Kosaka H et al. Identification and characterization of cell lines with a defect in a post-adsorption stage of Sendai virus-mediated membrane fusion. J Biol Chem 2000;275:17549–17555.

33 Tan HK, Toh CX, Ma D et al. Human finger-prick induced pluripotent stem cells facilitate the development of stem cell banking. STEM CELLS TRANSLATIONAL MEDICINE 2014;3:586–598.

See www.StemCellsTM.com for supporting information available online.

Prediction of interindividual differences in hepatic functions and drug sensitivity by using human iPS-derived hepatocytes

Kazuo Takayama[a,b,c], Yuta Morisaki[a], Shuichi Kuno[a], Yasuhito Nagamoto[a,c], Kazuo Harada[d], Norihisa Furukawa[a], Manami Ohtaka[e], Ken Nishimura[f], Kazuo Imagawa[a,c,g], Fuminori Sakurai[a,h], Masashi Tachibana[a], Ryo Sumazaki[g], Emiko Noguchi[i], Mahito Nakanishi[e], Kazumasa Hirata[d], Kenji Kawabata[j,k], and Hiroyuki Mizuguchi[a,b,c,l,1]

[a]Laboratory of Biochemistry and Molecular Biology; [b]iPS Cell-based Research Project on Hepatic Toxicity and Metabolism, [d]Laboratory of Applied Environmental Biology, [h]Laboratory of Regulatory Sciences for Oligonucleotide Therapeutics, Clinical Drug Development Project, and [k]Laboratory of Biomedical Innovation, Graduate School of Pharmaceutical Sciences, Osaka University, Osaka 565-0871, Japan; [c]Laboratory of Hepatocyte Regulation, and [j]Laboratory of Stem Cell Regulation, National Institute of Biomedical Innovation, Osaka 567-0085, Japan; [e]Research Center for Stem Cell Engineering, National Institute of Advanced Industrial Science and Technology, Ibaraki 305-8562, Japan; [f]Laboratory of Gene Regulation, [g]Department of Child Health, and [i]Department of Medical Genetics, Faculty of Medicine, University of Tsukuba, Ibaraki 305-8575, Japan; and [l]The Center for Advanced Medical Engineering and Informatics, Osaka University, Osaka 565-0871, Japan

Edited by Shinya Yamanaka, Kyoto University, Kyoto, Japan, and approved October 17, 2014 (received for review July 16, 2014)

Interindividual differences in hepatic metabolism, which are mainly due to genetic polymorphism in its gene, have a large influence on individual drug efficacy and adverse reaction. Hepatocyte-like cells (HLCs) differentiated from human induced pluripotent stem (iPS) cells have the potential to predict interindividual differences in drug metabolism capacity and drug response. However, it remains uncertain whether human iPSC-derived HLCs can reproduce the interindividual difference in hepatic metabolism and drug response. We found that cytochrome P450 (CYP) metabolism capacity and drug responsiveness of the primary human hepatocytes (PHH)-iPS-HLCs were highly correlated with those of PHHs, suggesting that the PHH-iPS-HLCs retained donor-specific CYP metabolism capacity and drug responsiveness. We also demonstrated that the interindividual differences, which are due to the diversity of individual SNPs in the CYP gene, could also be reproduced in PHH-iPS-HLCs. We succeeded in establishing, to our knowledge, the first PHH-iPS-HLC panel that reflects the interindividual differences of hepatic drug-metabolizing capacity and drug responsiveness.

human iPS cells | hepatocyte | CYP2D6 | personalized drug therapy | SNP

Drug-induced liver injury (DILI) is a leading cause of the withdrawal of drugs from the market. Human induced pluripotent stem cell (iPSC)-derived hepatocyte-like cells (HLCs) are expected to be useful for the prediction of DILI in the early phase of drug development. Many groups, including our own, have reported that the human iPS-HLCs have the ability to metabolize drugs, and thus these cells could be used to detect the cytotoxicity of drugs that are known to cause DILI (1, 2). However, to accurately predict DILI, it will be necessary to establish a panel of human iPS-HLCs that better represents the genetic variation of the human population because there are large interindividual differences in the drug metabolism capacity and drug responsiveness of hepatocytes (3). However, it remains unclear whether the drug metabolism capacity and drug responsiveness of human iPS-HLCs could reflect those of donor parental primary human hepatocytes (PHHs). To address this issue, we generated the HLCs differentiated from human iPSCs which had been established from PHHs (PHH-iPS-HLCs). Then, we compared the drug metabolism capacity and drug responsiveness of PHH-iPS-HLCs with those of their parental PHHs, which are genetically identical to the PHH-iPS-HLCs.

Interindividual differences of cytochrome P450 (CYP) metabolism capacity are closely related to genetic polymorphisms, especially single nucleotide polymorphisms (SNPs), in CYP genes (4). Among the various CYPs expressed in the liver, CYP2D6 is responsible for the metabolism of approximately a quarter of commercially used drugs and has the largest phenotypic variability, largely due to SNPs (5). It is known that certain alleles result in the poor metabolizer phenotype due to a decrease of CYP2D6 metabolism. Therefore, the appropriate dosage for drugs that are metabolized by CYP2D6, such as tamoxifen, varies widely among individuals (6). Indeed, in the 1980s, polymorphism in CYP2D6 appears to have contributed to the withdrawal of CYP2D6-metabolized drugs such as perhexiline from the market in many countries (7). If we could establish a panel of HLCs that better represents the diversity of genetic polymorphisms in the human population, it might be possible to determine the appropriate dosage of a drug for a particular individual. However, it is not known whether the drug metabolism capacity and drug responsiveness of HLCs reflect the genetic diversity, including SNPs, in CYP genes. Therefore, in this study we generated HLCs from several PHHs that have various SNPs on CYP2D6 and then compared the CYP2D6 metabolism capacity and responses to CYP2D6-metabolized drugs between the PHH-iPS-HLCs and parental PHHs.

Significance

We found that individual cytochrome P450 (CYP) metabolism capacity and drug sensitivity could be predicted by examining them in the primary human hepatocytes–human induced pluripotent stem cells–hepatocyte-like cells (PHH-iPS-HLCs). We also confirmed that interindividual differences of CYP metabolism capacity and drug responsiveness that are due to the diversity of individual single nucleotide polymorphisms in the CYP gene could also be reproduced in the PHH-iPS-HLCs. These findings suggest that interindividual differences in drug metabolism capacity and drug response could be predicted by using HLCs differentiated from human iPS cells. We believe that iPS-HLCs would be a powerful technology not only for accurate and efficient drug development, but also for personalized drug therapy.

Author contributions: K.T. and H.M. designed research; K.T., Y.M., and S.K. performed research; K.T., Y.M., Kazuo Harada, M.O., K.N., K.I., M.N., and Kazumasa Hirata contributed new reagents/analytic tools; K.T., Y.N., N.F., F.S., M.T., R.S., E.N., K.K., and H.M. analyzed data; and K.T. and H.M. wrote the paper.

The authors declare no conflict of interest.

This article is a PNAS Direct Submission.

Data deposition: The DNA microarray data reported in this paper have been deposited in the Gene Expression Omnibus (GEO) database, www.ncbi.nlm.nih.gov/geo (accession no. GSE61287).

[1]To whom correspondence should be addressed. Email: mizuguch@phs.osaka-u.ac.jp.

This article contains supporting information online at www.pnas.org/lookup/suppl/doi:10.1073/pnas.1413481111/-/DCSupplemental.

To this end, PHHs were reprogrammed into human iPSCs and then differentiated into the HLCs. To examine whether the HLCs could reproduce the characteristics of donor PHHs, we first compared the CYP metabolism capacity and response to a hepatotoxic drug between PHHs and genetically identical PHH-iPS-HLCs (12 donors were used in this study). Next, analyses of hepatic functions, including comparisons of the gene expression of liver-specific genes and CYPs, were performed to examine whether the hepatic characteristics of PHHs were reproduced in the HLCs. To the best of our knowledge, this is the first study to compare the functions between iPSC-derived cells from various donors and their parental cells with identical genetic backgrounds. Finally, we examined whether the PHH-iPS-HLCs exhibited a capacity for drug metabolism and drug responsiveness that reflect the genetic diversity such as SNPs on CYP genes.

Results

Reprogramming of PHHs to Human iPSCs. To examine whether the HLCs could reproduce interindividual differences in liver functions, we first tried to generate human iPSCs from the PHHs of 12 donors. PHHs were transduced with a Yamanaka 4 factor-expressing SeV (SeVdp-iPS) vector (*SI Appendix*, Fig. S1*A*) in the presence of SB431542, PD0325901, and a rock inhibitor, which could promote the somatic reprogramming (8). The reprogramming procedure is shown in *SI Appendix*, Fig. S1*B*. The human iPSCs generated from PHHs (PHH-iPSCs) were positive for alkaline phosphatase (*SI Appendix*, Fig. S1*B*, *Right*), NANOG, OCT4, SSEA4, SOX2, Tra1-81, and KLF4 (Fig. 1*A*). The gene expression levels of the pluripotent markers (*OCT3/4*, *SOX2*, and *NANOG*) in the PHH-iPSCs were approximately equal to those in human embryonic stem cells (ESCs) (*SI Appendix*, Fig. S1*C*, *Left*). The gene expression levels of the hepatic markers [*albumin (ALB)*, *CYP3A4*, and *αAT*] in the PHH-iPSCs were significantly lower than those in the parental PHHs (*SI Appendix*, Fig. S1*C*, *Right*). We also confirmed that the PHH-iPSCs have the ability to differentiate into the three embryonic germ layers in vitro by embryoid body formation and in vivo by teratoma formation (*SI Appendix*, Fig. S2 *A* and *B*, respectively). To verify that the PHH-iPSCs originated from PHHs, short tandem repeat analysis was performed in the PHH-iPSCs and parental PHHs (*SI Appendix*, Fig. S2*C*). The results showed that the PHH-iPSCs were indeed originated from PHHs. Taken together, these results indicated that the generation of human iPSCs from PHHs was successfully performed. It is known that a transient epigenetic memory of the original cells is retained in early-passage iPSCs, but not in late-passage iPSCs (9). To examine whether the hepatic differentiation capacity of PHH-iPSCs depends on their passage number, PHH-iPSCs having various passage numbers were differentiated into the hepatic lineage (Fig. 1*B*). The *tyrosine aminotransferase* (*TAT*) expression levels and albumin (ALB) secretion levels in early passage PHH-iPS-HLCs (fewer than 10 passages) were higher than those of late passage PHH-iPS-HLCs (more than 14 passages). These results suggest that the hepatic differentiation tendency is maintained in early passage PHH-iPSCs, but not in late passage PHH-iPSCs. In addition, the hepatic functions of late passage PHH-iPS-HLCs were similar to those in the HLCs derived from late passage non–PHH-derived iPS cells (such as dermal cells, blood cells, and Human Umbilical Vein Endothelial Cells (HUVEC)-derived iPS cells) (*SI Appendix*, Fig. S3). Therefore, PHH-iPSCs, which were passaged more than 20 times, were used in our study to avoid any potential effect of transient epigenetic memory retained in parental PHHs on hepatic functions.

HLCs Were Differentiated from PHH-iPSCs Independent of Their Differentiation Tendency. To compare the hepatic characteristics among the PHH-iPS-HLCs that were generated from PHHs of the 12 donors, all of the PHH-iPSCs were differentiated into the HLCs as described in Fig. 2*A*. However, the differences in hepatic function among PHH-iPS-HLCs could not be properly compared because there were large inter-PHH-iPSC line differences in the hepatic differentiation efficiency based on ALB or asialoglycoprotein receptor 1 (ASGR1) expression analysis (Fig. 2*B*). In addition, there were also large inter-PHH-iPS-HLC line differences in ALB or urea secretion capacities (Fig. 2*C*). These results suggest that it is impossible to compare the hepatic characteristics among PHH-iPS-HLCs without compensating for the differences in the hepatic differentiation efficiency. Recently, we developed a method to maintain and proliferate the hepatoblast-like cells (HBCs) generated from human ESCs/iPSCs by using human laminin 111 (LN111) (10). To examine whether the hepatic differentiation efficiency could be made uniform by generating the HLCs following purification and proliferation of the HBCs, the PHH-iPS-HBCs were cultured on LN111 as

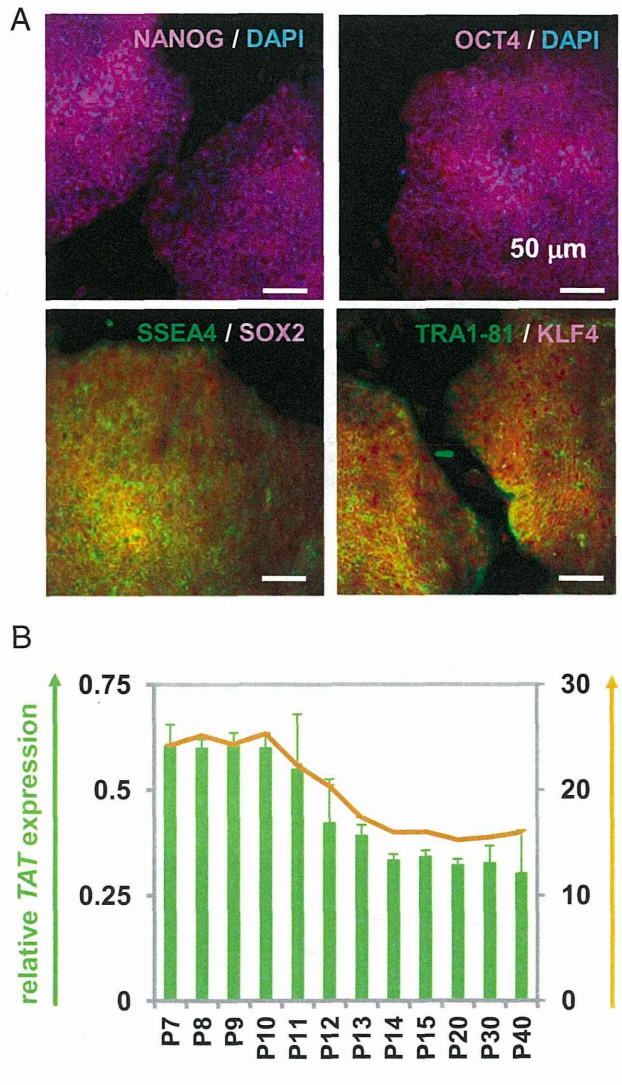

Fig. 1. Establishment and characterization of human iPSCs generated from PHHs. (*A*) The PHH-iPSCs were subjected to immunostaining with anti-NANOG (red), OCT4 (red), SSEA4 (green), SOX2 (red), TRA1-81 (green), and KLF4 (red) antibodies. Nuclei were counterstained with DAPI (blue) (*Upper*). (*B*) The *TAT* expression and ALB secretion levels in the PHH-iPS-HLCs (P7–P40) were examined. On the *y* axis, the gene expression level of *TAT* in PHHs was taken as 1.0.

CELL BIOLOGY

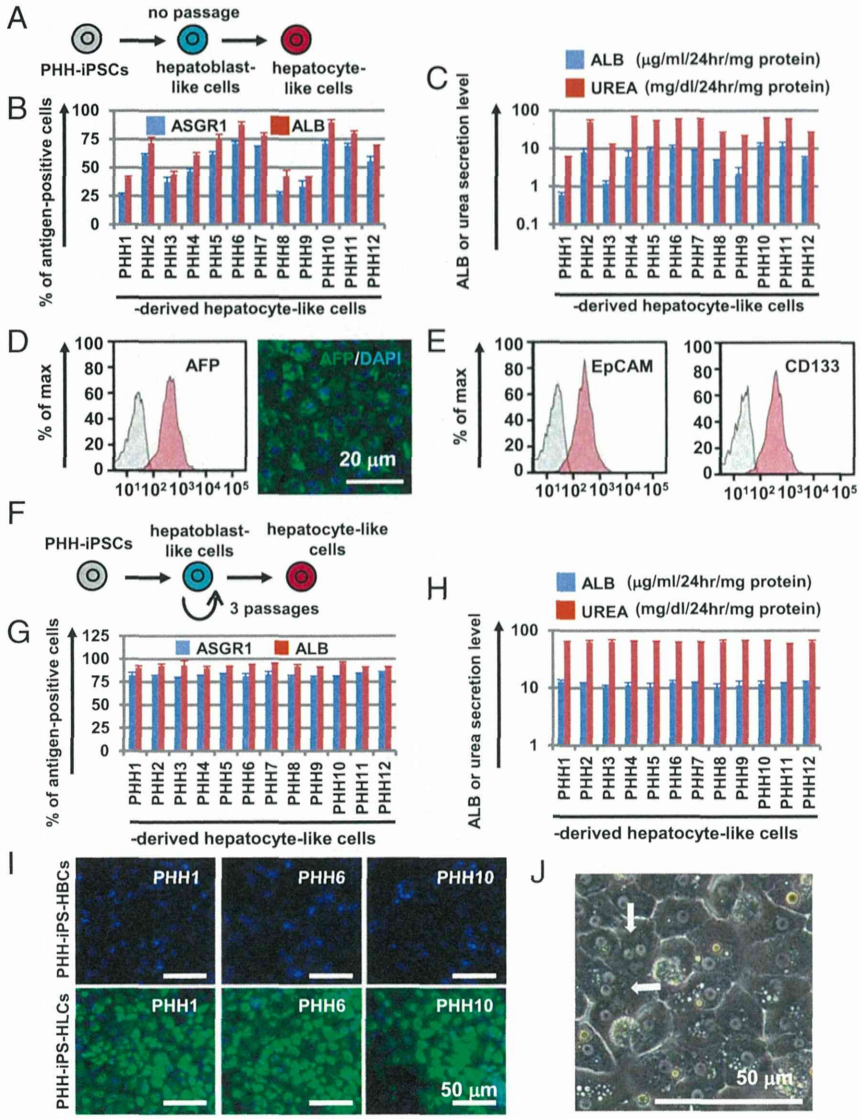

Fig. 2. Highly efficient hepatocyte differentiation from PHH-iPSCs independent of their differentiation tendency. (*A*) PHH-iPSCs were differentiated into the HLCs via the HBCs. (*B*) On day 25 of differentiation, the efficiency of hepatocyte differentiation was measured by estimating the percentage of ASGR1- or ALB-positive cells using FACS analysis. (*C*) The amount of ALB or urea secretion was examined in PHH-iPS-HLCs. (*D*) The percentage of AFP-positive cells in PHH-iPS-HBCs was examined by using FACS analysis (*Left*). The PHH-iPS-HBCs were subjected to immunostaining with anti-AFP (green) antibodies. Nuclei were counterstained with DAPI (blue) (*Right*). (*E*) The percentage of EpCAM- and CD133-positive cells in PHH-iPS-HBCs was examined by using FACS analysis (*Left*). (*F*) PHH-iPSCs were differentiated into the hepatic lineage, and then PHH-iPS-HBCs were purified and maintained for three passages on human LN111. Thereafter, expanded PHH-iPS-HBCs were differentiated into the HLCs. (*G*) The efficiency of hepatic differentiation from PHH-iPS-HBCs was measured by estimating the percentage of ASGR1- or ALB-positive cells using FACS analysis. (*H*) The amount of ALB or urea secretion in PHH-iPS-HLCs was examined. Data represent the mean ± SD from three independent differentiations. (*I*) The PHH1-, 6-, or 10-iPS-HBCs and -HLCs were subjected to immunostaining with anti-αAT (green) antibodies. Nuclei were counterstained with DAPI (blue). (*J*) A phase-contrast micrograph of PHH-iPS-HLCs.

previously described (10), and then differentiated into the HLCs. Almost all of the cells were positive for the hepatoblast marker [alpha-fetoprotein (AFP)] (Fig. 2*D*). In addition, the PHH-iPS-HBCs were positive for two other hepatoblast markers, EpCAM and CD133 (Fig. 2*E*). To examine the hepatic differentiation efficiency of the PHH-iPS-HBCs maintained on LN111-coated dishes for three passages (Fig. 2*F*), the HBCs were differentiated into the HLCs, and then the percentage of ALB- and ASGR1-positive cells was measured by FACS analysis (Fig. 2*G*). All 12 PHH-iPS-HBCs could efficiently differentiate into the HLCs, yielding more than 75% or 85% ASGR1- or ALB-positive cells, respectively. In addition, there was little difference between the PHH-iPSC lines in ALB or urea secretion capacities (Fig. 2*H*). Although there were large differences in the hepatic differentiation capacity among the PHH1/6/10 (Fig. 2*B*), PHH1/6/10-iPS-HBCs could efficiently differentiate into the HLCs that homogeneously expressed αAT (Fig. 2*I*). After the hepatic differentiation of the PHH-iPS-HBCs, the morphology of the HLCs was similar to that of the PHHs: polygonal with distinct round binuclei (Fig. 2*J*). These results indicated that the hepatic differentiation efficiency of the 12 PHH-iPSC lines could be rendered uniform by inducing hepatic maturation after the establishment of self-renewing HBCs. Therefore, we expected that differences in the hepatic characteristics among the HLCs generated from the 12 individual donor PHH-iPS-HBCs could be properly compared. In addition, the hepatic differentiation efficiency could be rendered uniform not only in the PHH-iPSC lines but also in non–PHH-iPSC lines and human ESCs by performing hepatic maturation after the establishment of self-renewing HBCs (*SI Appendix*, Fig. S4). In Figs. 3 and 4, the HLCs were differentiated after the HBC proliferation step to normalize the hepatic differentiation efficiency.

PHH-iPS-HLCs Retained Donor-Specific Drug Metabolism Capacity and Drug Responsiveness. To examine whether the hepatic functions of individual PHH-iPS-HLCs reflect those of individual PHHs, the CYP metabolism capacity and drug responsiveness of PHH-iPS-HLCs were compared with those of PHHs. PHHs are often used as a positive control to assess the hepatic functions of the HLCs, although in all of the previous reports, the donor of PHHs has been different from that of human iPSCs. Because it is generally considered that CYP activity differs widely among individuals, the hepatic functions of the HLCs should be compared with those of genetically identical PHHs to accurately evaluate the hepatic functions of the HLCs. The CYP1A2, -2C9, and -3A4 activity levels in the PHH-iPS-HLCs were ~60% of

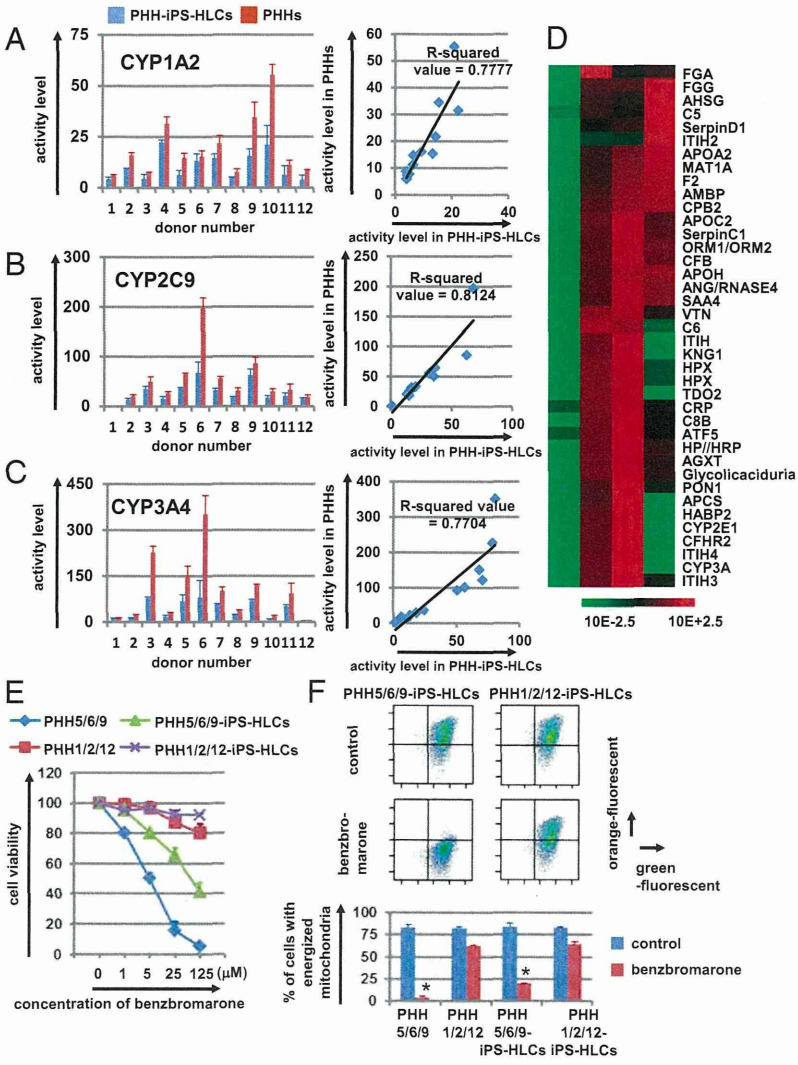

Fig. 3. The drug metabolism capacity and drug responsiveness of PHH-iPS-HLCs were highly correlated with those of their parental PHHs. (*A–C*) CYP1A2 (*A*), -2C9 (*B*), and -3A4 (*C*) activity levels in PHH-iPS-HLCs and PHHs were measured by LC-MS/MS analysis. The R-squared values are indicated in each figure. (*D*) The global gene expression analysis was performed in PHH9-iPSCs, PHH9-iPS-HLCs, PHH9s, and HepG2 (PHH-iPSCs, PHH-iPS-HLCs, and PHHs are genetically identical). Heat-map analyses of liver-specific genes are shown. (*E*) The cell viability of PHH5/6/9, PHH1/2/12, PHH5/6/9-iPS-HLCs, and PHH1/2/12-iPS-HLCs was examined after 24 h exposure to different concentrations of benzbromarone. The cell viability was expressed as a percentage of that in the cells treated only with solvent. (*F*) The percentage of cells with energized mitochondria in the DMSO-treated (control, *Upper*) or benzbromarone-treated (*Lower*) cells based on FACS analysis. Double-positive cells (green+/orange+) represent energized cells, whereas single-positive cells (green+/orange–) represent apoptotic and necrotic cells. Data represent the mean ± SD from three independent experiments (*Lower Graph*). Student *t* test indicated that the percentages in the "control" were significantly higher than those in the "benzbromarone" group ($P < 0.01$). The "PHH5/6/9" represents the average value of cell viability (*E*) or mitochondrial membrane potential (*F*) in PHH5, PHH6, and PHH9. The "PHH1/2/12" represents the average value of cell viability or mitochondrial membrane potential in PHH1, PHH2, and PHH12. PHH5, PHH6, and PHH9 were the top three with respect to CYP2C9 activity levels, whereas PHH1, PHH2, and PHH12 had the lowest CYP2C9 activity levels.

those in the PHHs (Fig. 3 *A–C* and *SI Appendix*, Fig. S5). Interestingly, the CYP1A2, -2C9, and -3A4 activity levels in the PHH-iPS-HLCs were highly correlated with those in the PHHs (the R-squared values were more than 0.77) (Fig. 3 *A*, *B*, and *C*, respectively). These results suggest that it would be possible to predict the individual CYP activity levels through analysis of the CYP activity levels of the PHH-iPS-HLCs. Because the average and variance of CYP3A4 activity levels in PHH-iPS-HLCs, non–PHH-iPS-HLCs, and human ES-HLCs were similar to each other (*SI Appendix*, Fig. S6), the drug metabolism capacity of PHH-iPS-HLCs might be similar to that of nonliver tissue-derived iPS-HLCs and human ES-HLCs. Therefore, it might be possible to predict the diversity of drug metabolism capacity among donors by using nonliver tissue-derived iPS-HLCs and human ES-HLCs as well as PHH-iPS-HLCs. On the other hand, the CYP induction capacities of PHH-iPS-HLCs were weakly correlated with those of PHHs (*SI Appendix*, Fig. S7 *A–C*). To further investigate the characteristics of the HLCs, DNA microarray analyses were performed in genetically identical undifferentiated iPSCs, PHH-iPS-HLCs, and PHHs. The gene expression patterns of liver-specific genes, CYPs, and transporters in the PHH-iPS-HLCs were similar to those in PHHs (Fig. 3*D* and *SI Appendix*, Fig. S7 *D* and *E*, respectively). Next, the hepatotoxic drug responsiveness of PHH-iPS-HLCs was compared with that of PHHs. Benzbromarone, which is known to cause hepatotoxicity by CYP2C9 metabolism (11), was treated to PHH5/6/9 and PHH5/6/9-iPS-HLCs, which have high CYP2C9 activity, or PHH1/2/12 and PHH1/2/12-iPS-HLCs which have low CYP2C9 activity (Fig. 3*E*). The susceptibility of the PHH5/6/9 and PHH5/6/9-iPS-HLCs to benzbromarone was higher than that of PHH1/2/12 and PHH1/2/12-iPS-HLCs, respectively. These results were attributed to the higher CYP2C9 activity levels in PHH5/6/9 and PHH5/6/9-iPS-HLCs compared with those in PHH1/2/12 and PHH1/2/12-iPS-HLCs. Because it is also known that benzbromarone causes mitochondrial toxicity (12), an assay of mitochondrial membrane potential was performed in benzbromarone-treated PHHs and PHH-iPS-HLCs (Fig. 3*F*). The mitochondrial toxicity observed in PHH5/6/9 and PHH5/6/9-iPS-HLCs was more severe than that in PHH1/2/12 and PHH1/2/12-iPS-HLCs, respectively. Taken together, these results suggest that the hepatic functions of the individual PHH-iPS-HLCs were highly correlated with those of individual PHHs.

Interindividual Differences in CYP2D6-Mediated Metabolism and Drug Toxicity, Which Are Caused by SNPs in CYP2D6, Are Reproduced in the PHH-iPS-HLCs. Because certain SNPs are known to have a large impact on CYP activity, the genetic variability of CYP plays an important role in interindividual differences in drug response. CYP2D6 shows the large phenotypic variability due to genetic polymorphism (13). We next examined whether the PHHs used

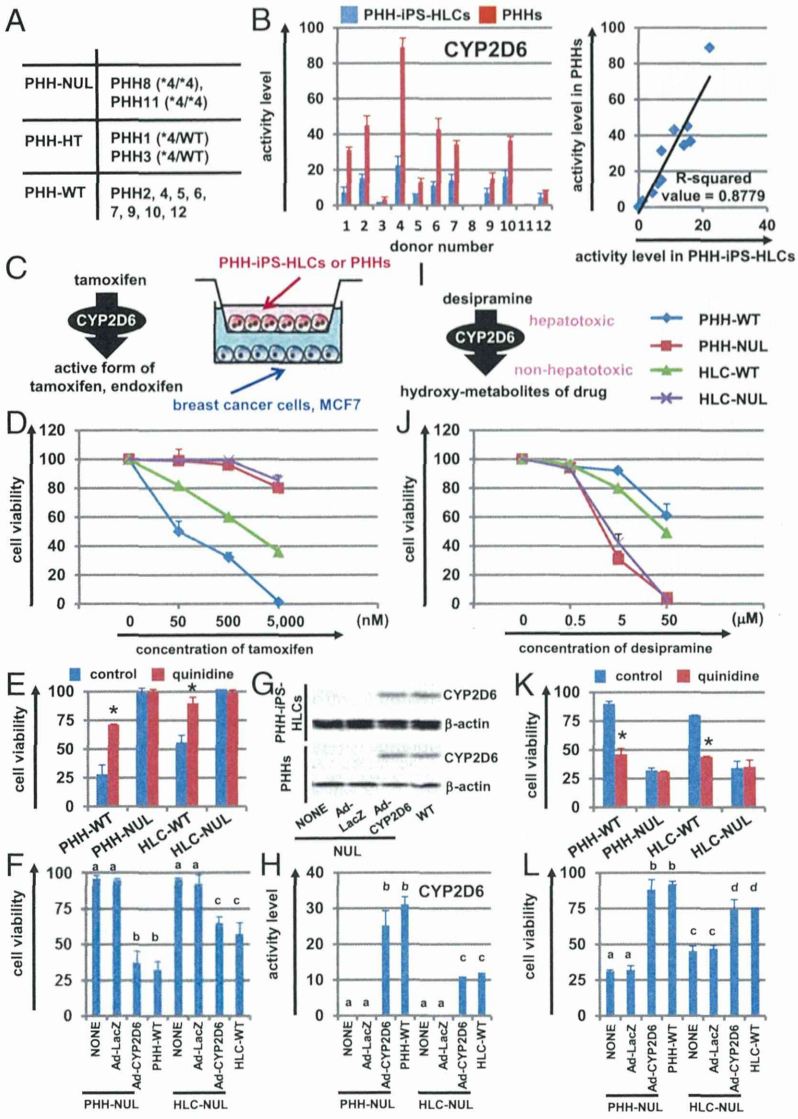

Fig. 4. The interindividual differences in CYP2D6 metabolism capacity and drug responsiveness induced by SNPs in CYP2D6 are reproduced in the PHH-iPS-HLCs. (*A*) SNPs (CYP2D6*3, *4, *5, *6, *7, *8, *16, and *21) in the CYP2D6 gene were analyzed. (*B*) The CYP2D6 activity levels in PHH-iPS-HLCs and PHHs were measured by LC-MS/MS analysis. (*C*) The pharmacological activity of tamoxifen-dependent conversion to its metabolite, endoxifen, by the CYP2D6. The coculture system of breast cancer cells (MCF-7 cells) and the PHH-iPS-HLCs are illustrated. (*D*) The cell viability of MCF-7 cells was assessed after 72-h exposure to different concentrations of tamoxifen. (*E*) The cell viability of MCF-7 cells, which were cocultured with PHH-WT, PHH-NUL, HLC-WT, and HLC-NUL, was assessed after 72-h exposure to 500 nM of tamoxifen in the presence or absence of 3 nM quinidine (a CYP2D6 inhibitor). (*F*) The cell viability of MCF-7 cells cocultured with Ad-CYP2D6-transduced PHH-NUL and HLC-NUL was examined after 72-h exposure to 500 nM of tamoxifen. (*G* and *H*) The CYP2D6 expression (*G*) and activity (*H*) levels in Ad-CYP2D6-transduced PHH-NUL and HLC-NUL were examined by Western blotting and LC-MS/MS analysis. (*I*) The detoxification of desipramine-dependent conversion to its conjugated form by the CYP2D6. (*J*) The cell viability of PHH-WT, PHH-NUL, HLC-WT, and HLC-NUL was assessed after 24-h exposure to different concentrations of desipramine. (*K*) The cell viability of the PHH-WT and HLC-WT was assessed after 24-h exposure to 5 μM of desipramine in the presence or absence of 5 μM of quinidine (a CYP2D6 inhibitor). (*L*) The cell viability of the Ad-CYP2D6-transduced PHH-NUL and HLC-NUL was examined after 24-h exposure to 5 μM of desipramine. The cell viability was expressed as a percentage of that in the cells treated with only solvent. Data represent the mean ± SD from three independent experiments. In *E* and *K*, Student *t* test indicated that the cell viability in the "control" was significantly higher than that in the "quinidine" group ($P < 0.01$). In *F*, *H*, and *L*, statistical significance was evaluated by ANOVA followed by Bonferroni post hoc tests to compare all groups. Groups that do not share the same letter are significantly different from each other ($P < 0.05$).

in this study have the CYP2D6 poor metabolizer genotypes (CYP2D6 *3, *4, *5, *6, *7, *8, *16, and *21) (5). PHH8 and -11 have CYP2D6*4 (null allele), whereas the others have a wild type (WT) or hetero allele (*SI Appendix*, Table S3 and Fig. 4*A*). Consistent with this finding, the PHH8/11-iPS-HLCs also have CYP2D6*4, whereas the others have a wild type or hetero allele. As expected, the CYP2D6 activity levels in the PHH8/11 (PHH-NUL) and PHH8/11-iPS-HLC (HLC-NUL) were significantly lower than those in the PHH-WT and HLC-WT, respectively (Fig. 4*B*). The pharmacological activity of tamoxifen, which is the most widely used agent for patients with breast cancer, is dependent on its conversion to its metabolite, endoxifen, by the CYP2D6 (Fig. 4*C*). To examine whether the pharmacological activity of tamoxifen could be predicted by using PHHs and HLCs that have either the null type CYP2D6*4 allele or wild-type CYP2D6 allele, the breast cancer cell line MCF7 was cocultured with PHHs or HLCs, and then the cells were treated with tamoxifen (Fig. 4*D*). The cell viability of MCF7 cells cocultured with PHHs-NUL or HLCs-NUL was significantly higher than that of MCF7 cells cocultured with PHHs-WT or HLCs-WT. The decrease in cell viability of MCF7 cells cocultured with PHHs-WT or HLCs-WT was rescued by treatment with a CYP2D6 inhibitor, quinidine (Fig. 4*E*). We also confirmed that the cell viability of MCF7 cells cocultured with PHHs-NUL or HLCs-NUL was decreased by CYP2D6 overexpression in the PHHs-NUL or HLCs-NUL (Fig. 4*F*). Note that the expression (Fig. 4*G*) and activity (Fig. 4*H*) levels of CYP2D6 in CYP2D6-expressing adenovirus vector (Ad-CYP2D6)-transduced PHHs-NUL or HLCs-NUL were comparable to those of PHHs-WT or HLCs-WT. These results indicated that the PHHs-WT and HLCs-WT could more efficiently metabolize tamoxifen than the PHHs-NUL and HLCs-NUL, respectively, and thereby induced higher toxicity in MCF7 cells. Similar results were obtained with the other breast cancer cell line, T-47D (*SI Appendix*, Fig. S8 *A–D*). Next, we examined whether the CYP2D6-mediated drug-induced hepatotoxicity could be predicted by using PHHs and HLCs having either a null type CYP2D6*4 allele or wild-type CYP2D6 allele. PHHs and HLCs were treated with desipramine, which is known to cause hepatotoxicity (Fig. 4*I*) (14). The cell viability of PHHs-NUL and HLCs-NUL was significantly lower than that of PHHs-WT and HLCs-WT (Fig. 4*J*). The cell viability of the PHHs-WT or HLCs-WT was decreased by treatment with a CYP2D6 inhibitor, quinidine (Fig. 4*K*). We also confirmed that the decrease in the cell viability of the PHHs-NUL or HLCs-NUL was rescued by CYP2D6 overexpression in the PHHs-NUL or HLCs-NUL (Fig. 4*L*). Similar

results were obtained with the other hepatotoxic drug, perhexiline (*SI Appendix*, Fig. S8 *E–H*). These results indicated that the PHHs-WT and HLCs-WT could more efficiently metabolize imipramine and thereby reduce toxicity compared with the PHHs-NUL and HLCs-NUL. Taken together, our findings showed that the interindividual differences in CYP metabolism capacity and drug responsiveness, which are prescribed by an SNP in genes encoding CYPs, were also reproduced in the PHH-iPS-HLCs.

Discussion

The purpose of this study was to examine whether the individual HLCs could reproduce the hepatic function of individual PHHs. A Yamanaka 4 factor-expressing SeV vector was used in this study to generate integration-free human iPSCs from PHHs. It is known that SeV vectors can express exogenous genes without chromosomal insertion, because these vectors replicate their genomes exclusively in the cytoplasm (15). To examine the different cellular phenotypes associated with SNPs in human iPSC derivatives, the use of integration-free human iPSCs is essential.

We found that the CYP activity levels of the PHH-iPS-HLCs reflected those of parent PHHs, as shown in Fig. 3 *A–C*. There were few interindividual differences in the ratio of CYP expression levels in the PHH-iPS-HLCs to those in PHHs (*SI Appendix*, Fig. S5). Together, these results suggest that it is possible to predict the individual CYP activity levels through analysis of the CYP activity levels of the PHH-iPS-HLCs. In the future, it will be necessary to confirm these results in skin or blood cell-derived iPSCs as well as PHH-iPSCs, although donor-matched PHHs and blood cells (or skin cells) are difficult to obtain. In addition, the comparison of hepatic functions between genetically identical PHHs and PHH-iPS-HLCs (Fig. 3 *A–C*) would enable us to accurately ascertain whether the HLCs exhibit sufficient hepatic function to be a suitable substitute for PHHs in the early phase of pharmaceutical development. Because the drug responsiveness of the individual HLCs reflected that of individual PHHs (Fig. 3 *E* and *F*), it might be possible to perform personalized drug therapy following drug screening using a patient's HLCs. However, the R-squared values of the individual CYP activities differed from each other (Fig. 3 *A–C*), suggesting that the activity levels of some CYPs are largely influenced not only by genetic information but also by environmental factors, such as dietary or smoking habits.

The interindividual differences of CYP2D6 metabolism capacity and drug responsiveness that were prescribed by SNP in genes encoding CYP2D6 were reproduced in the PHH-iPS-HLCs (Fig. 4). It was impossible to perform drug screening in the human hepatocytes derived from a donor with rare SNPs because these hepatocytes could not be obtained. However, because human iPSCs can be generated from such donors with rare SNPs, the CYP metabolism capacity and drug responsiveness of these donors might be possible to predict. Further, it would also be possible to identify the novel SNP responsible for an unexpected hepatotoxicity by using the HLCs in which whole genome sequences are known. We thus believe that the HLCs will be a powerful tool not only for accurate and efficient drug development but also for personalized drug therapy.

Experimental Procedures

DNA Microarray. Total RNA was prepared from the PHH9-iPSCs, PHH9-iPS-HLCs, PHH9, and human hepatocellular carcinoma cell lines by using an RNeasy Mini kit. A pool of three independent samples was used in this study. cRNA amplifying, labeling, hybridizing, and analyzing were performed at Miltenyi Biotec. The Gene Expression Omnibus (GEO) accession no. for the microarray analysis is GSE61287.

Flow Cytometry. Single-cell suspensions of human iPSC-derived cells were fixed with 2% (vol/vol) paraformaldehyde (PFA) for 20 min, and then incubated with the primary antibody (described in *SI Appendix*, Table S1), followed by the secondary antibody (described in *SI Appendix*, Table S2). In case of the intracellular staining, the Permeabilization Buffer (eBioscience) was used to create holes in the membrane thereby allowing the antibodies to enter the cell effectively. Flow cytometry analysis was performed using a FACS LSR Fortessa flow cytometer (BD Biosciences).

ACKNOWLEDGMENTS. We thank Yasuko Hagihara, Natsumi Mimura, and Shigemi Isoyama for their excellent technical support. H.M. and K.K. were supported by grants from the Ministry of Health, Labor, and Welfare. H.M. was also supported by the Project for Technological Development, Research Center Network for Realization of Regenerative Medicine of the Japan Science and Technology Agency and by the Uehara Memorial Foundation. F.S. was supported by the Program for Promotion of Fundamental Studies in Health Sciences of the National Institute of Biomedical Innovation. K.T. and Y.N. were supported by a grant-in-aid for the Japan Society for the Promotion of Science Fellows.

1. Takayama K, et al. (2012) Efficient generation of functional hepatocytes from human embryonic stem cells and induced pluripotent stem cells by HNF4α transduction. *Mol Ther* 20(1):127–137.
2. Medine CN, et al. (2013) Developing high-fidelity hepatotoxicity models from pluripotent stem cells. *Stem Cells Transl Med* 2(7):505–509.
3. Ingelman-Sundberg M (2004) Pharmacogenetics of cytochrome P450 and its applications in drug therapy: The past, present and future. *Trends Pharmacol Sci* 25(4): 193–200.
4. Ingelman-Sundberg M (2001) Genetic susceptibility to adverse effects of drugs and environmental toxicants. The role of the CYP family of enzymes. *Mutat Res* 482(1-2): 11–19.
5. Zhou SF (2009) Polymorphism of human cytochrome P450 2D6 and its clinical significance: Part I. *Clin Pharmacokinet* 48(11):689–723.
6. Borges S, et al. (2006) Quantitative effect of CYP2D6 genotype and inhibitors on tamoxifen metabolism: Implication for optimization of breast cancer treatment. *Clin Pharmacol Ther* 80(1):61–74.
7. Bakke OM, Manocchia M, de Abajo F, Kaitin KI, Lasagna L (1995) Drug safety discontinuations in the United Kingdom, the United States, and Spain from 1974 through 1993: A regulatory perspective. *Clin Pharmacol Ther* 58(1):108–117.
8. Lin T, et al. (2009) A chemical platform for improved induction of human iPSCs. *Nat Methods* 6(11):805–808.
9. Polo JM, et al. (2010) Cell type of origin influences the molecular and functional properties of mouse induced pluripotent stem cells. *Nat Biotechnol* 28(8):848–855.
10. Takayama K, et al. (2013) Long-term self-renewal of human ES/iPS-derived hepatoblast-like cells on human laminin 111-coated dishes. *Stem Cell Reports* 1(4):322–335.
11. McDonald MG, Rettie AE (2007) Sequential metabolism and bioactivation of the hepatotoxin benzbromarone: Formation of glutathione adducts from a catechol intermediate. *Chem Res Toxicol* 20(12):1833–1842.
12. Kaufmann P, et al. (2005) Mechanisms of benzarone and benzbromarone-induced hepatic toxicity. *Hepatology* 41(4):925–935.
13. Ingelman-Sundberg M (2005) Genetic polymorphisms of cytochrome P450 2D6 (CYP2D6): Clinical consequences, evolutionary aspects and functional diversity. *Pharmacogenomics J* 5(1):6–13.
14. Spina E, et al. (1997) Relationship between plasma desipramine levels, CYP2D6 phenotype and clinical response to desipramine: A prospective study. *Eur J Clin Pharmacol* 51(5):395–398.
15. Nishimura K, et al. (2011) Development of defective and persistent Sendai virus vector: A unique gene delivery/expression system ideal for cell reprogramming. *J Biol Chem* 286(6):4760–4771.

Figure 1. FBL is highly expressed in pluripotent ES cells. Mouse ES cells were cultured for 10 days in the presence (+LIF) or absence of LIF (-LIF) and analyzed for pluripotency marker protein expression. (A) Alkaline phosphatase staining. ES cells cultured in the presence of LIF formed tightly packed colonies and had high alkaline phosphatase activity (upper panel), whereas ES cells cultured in the absence of LIF for 10 days showed flattened morphology and lower alkaline phosphatase activity (lower panel). (B) qRT-PCR analysis of *FBL* mRNA. The ES cells were cultured as in (A) for 10 days. (C) Western blot analysis of FBL, Nanog, and Oct4 expression. (D) Relative densitometric values of the bands. Values were normalized to α-tubulin. Expression levels of FBL, Nanog, and Oct4 in (C) cultured without LIF for 10 days were approximately 36%, 24%, and 30% of that of the cells cultured with LIF, respectively. (E) Immunofluorescence staining of FBL, Nanog, Oct4, and SSEA-1. The ES cells were cultured as in (A) for 10 days. (F) Localization of FBL in pluripotent and differentiated cells. Arrowheads indicate immunoreactivity of FBL in the nucleus. $*p < 0.01$ in (B, D). Scale bars: (A), 300 μm; (E), 30 μm; (F), 20 μm.

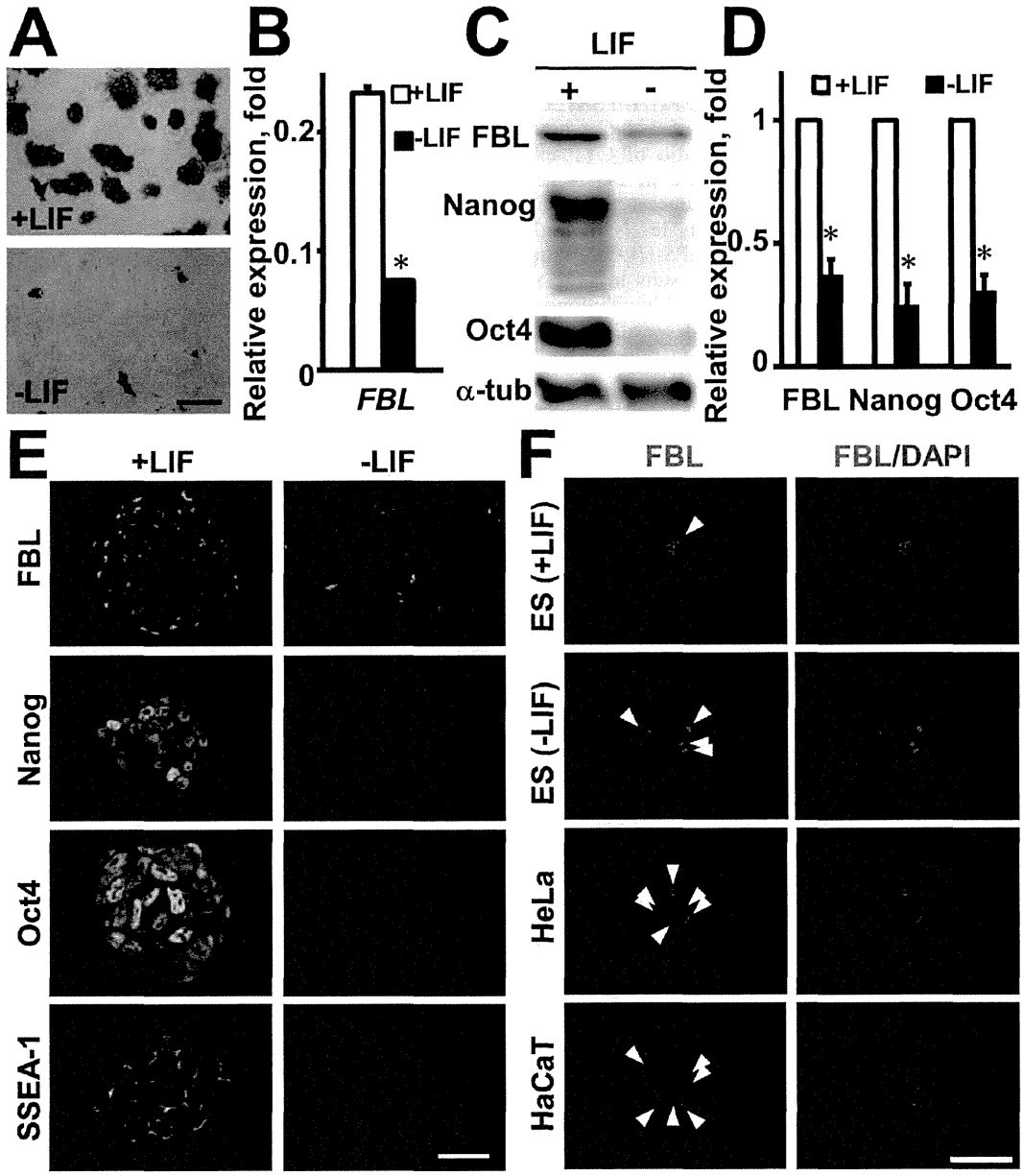

Figure 2. Stable expression of FBL prolongs the pluripotency of ES cells in the absence of LIF. ES cells stably expressing FBL or the control vector were cultured for 10 days in the presence or absence of LIF, and the expression levels of pluripotency-specific markers were analyzed. (A) Alkaline phosphatase staining of ES cells stably expressing FBL. (B) Western blot analysis of Nanog, Oct4, FBL, and FLAG antibodies. (C) Immunofluorescence analysis of ES cells with Nanog, Oct4, and SSEA-1 antibodies after culturing without LIF for 10 days. (D, E) FBL enhances reprogramming efficiency of MEFs. (D) Alkaline phosphatase staining of iPS cells induced with retroviruses for 4 transcription factors (Oct4, Sox2, Klf4, and cMyc) or 3 transcription factors (Oct4, Sox2, and Klf4) with or without FBL expression virus. Empty vector pMYs virus was used as control. (E) The colony numbers of iPS cells were counted and normalized to that of the control. Induction of iPS cells was assayed three times independently. Scale bars: (A), 200 μm; (C), 30 μm.

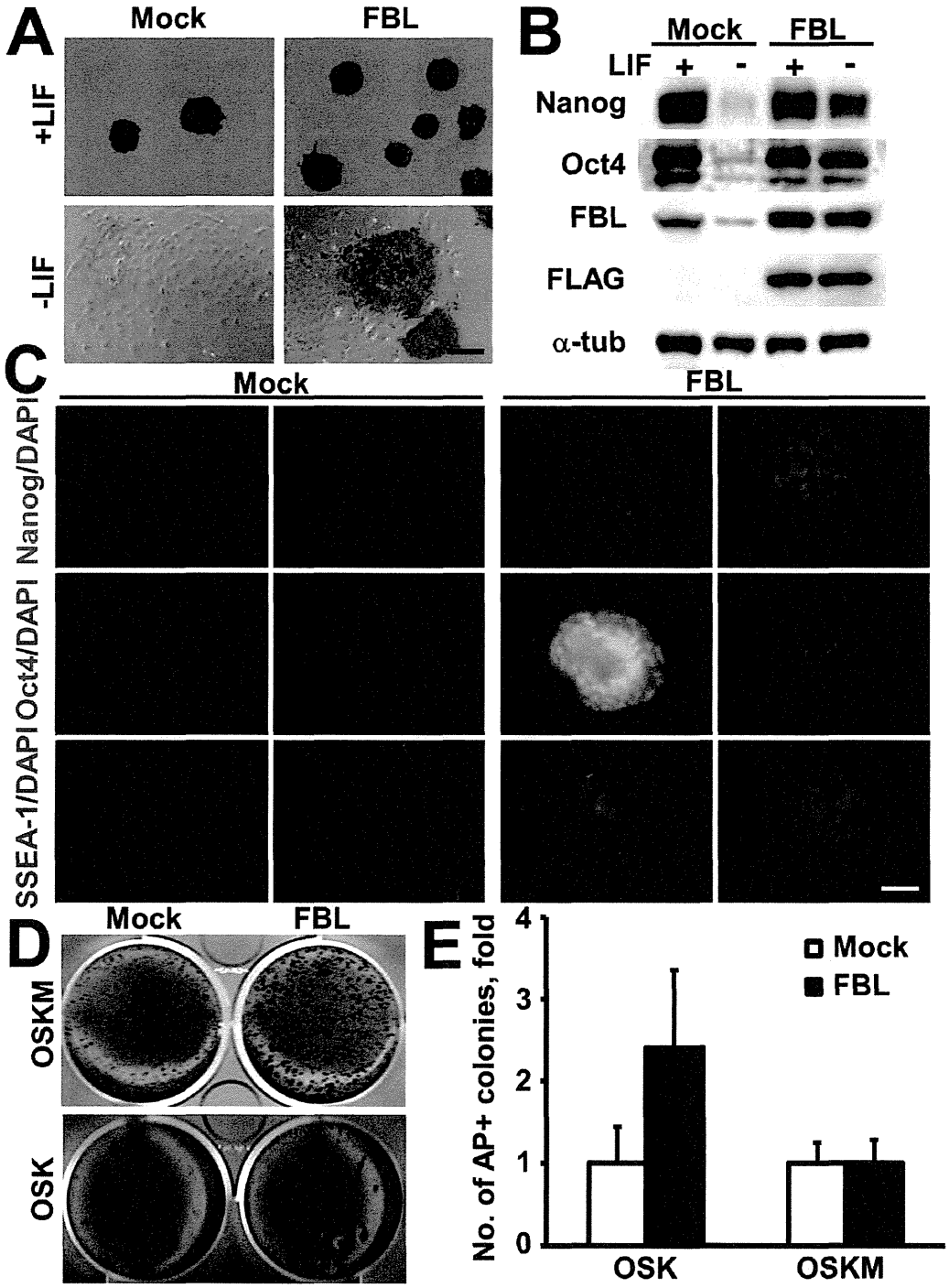

Figure 3. FBL is indispensable for the survival of ES cells. Tc-inducible FBL miRNA-expressing mouse ES cell lines were established and analyzed. (A) Immunofluorescence analysis of FBL expression. Upon withdrawal of Tc, FBL expression was notably decreased (middle and right). Cells were immunostained after 2 days of culture in the absence of Tc. (B) Western blot analysis of FBL expression in (A). A control miRNA did not affect the expression of FBL. (C) Morphological changes in FBL-knockdown ES cells under feeder-free culture conditions. After induction of FBL miRNA (-Tc), colonies of ES cells decreased in size and number at day 3, and had gradually disappeared by day 7. (D) Quantification of (C) by counting cell numbers after 3 days of culture. The data for control miRNA was shown on the left. (E) Significant increase in the number of TUNEL- or activated caspase-positive cells among FBL-knockdown ES cells cultured for 2 days in the absence of Tc. (F) Quantification of TUNEL-positive cells in (E). (G) Activated caspase staining of ES cells. GFP expression indicates the transfected cells with either GFP-control miRNA or GFP-FBL miRNA expression vector. (H) Apoptotic cell death caused by FBL-knockdown was significant in ES cells but not in other cell lines. Quantification of activated caspase-positive cells was performed 2 days after transfection with GFP-control miRNA or GFP-FBL miRNA expression vector. (I) Quantification of caspase-positive cells in ES cells. In the presence of LIF, ES cells were cultured with or without Tc for 2 days. In the absence of LIF, ES cells were pre-cultured in the presence of Tc for 7 days, further cultured with or without Tc for 2 days, and percentage of caspase-positive cells were analyzed. $*p < 0.01$ in (D, F, and H). $*p < 0.05$ in (I). Scale bars: (A), 30 μm; (C), 300 μm; (E, G), 50 μm.

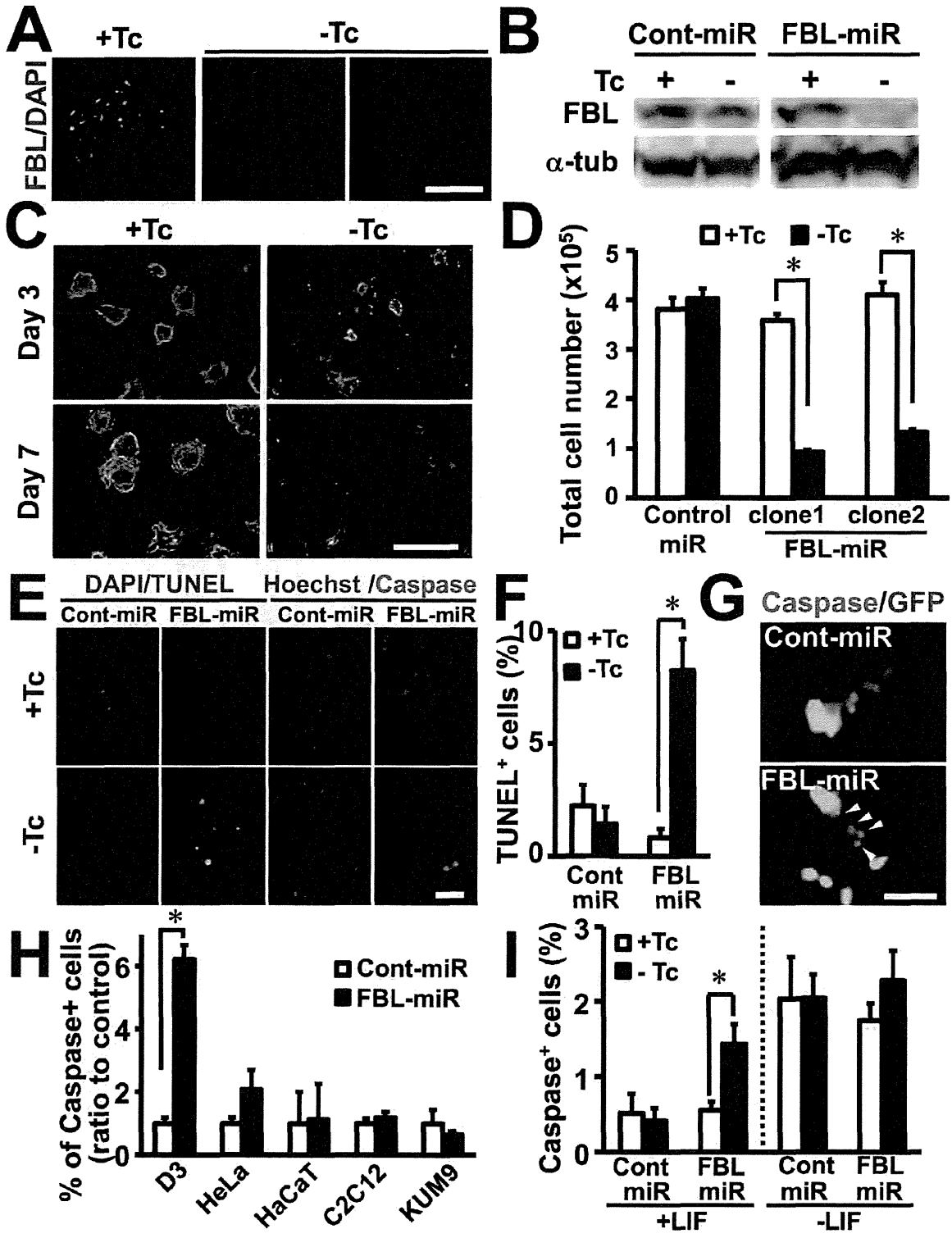

Figure 4. Knockdown of FBL in ES cells disturbs normal processing of pre-rRNA. (A, B) Pulse-chase labeling of ES cells with [^{3}H]-uridine. The ES cells were cultured with or without Tc for 2 days before labeling. (A) Autoradiography of total RNAs. The levels of 41S and 36S intermediate products and mature rRNA, 28S and 18S, were decreased in FBL-knockdown ES cells (-Tc). (B) Quantification of rRNA processing products. Each band was measured and divided by the sum of all products. Intermediate products, 47S/45S pre-rRNA and 34S/32S, were accumulated under FBL-knockdown conditions compared to control conditions. In contrast, the levels of mature forms of rRNA, 18S and 28S, were decreased under FBL-knockdown conditions. (C, D) Pulse-chase labeling with [methyl-^{3}H]-methionine. (C) Autoradiography of total RNAs. As in the case of [^{3}H]-uridine labeling, the levels of 41S and 36S intermediate products were decreased under FBL-knockdown conditions. (D) Quantification of methylated rRNA products. Graph shows the comparison of relative densitometric values of methylated rRNA products. Each experiment was performed two times and the data were averaged.

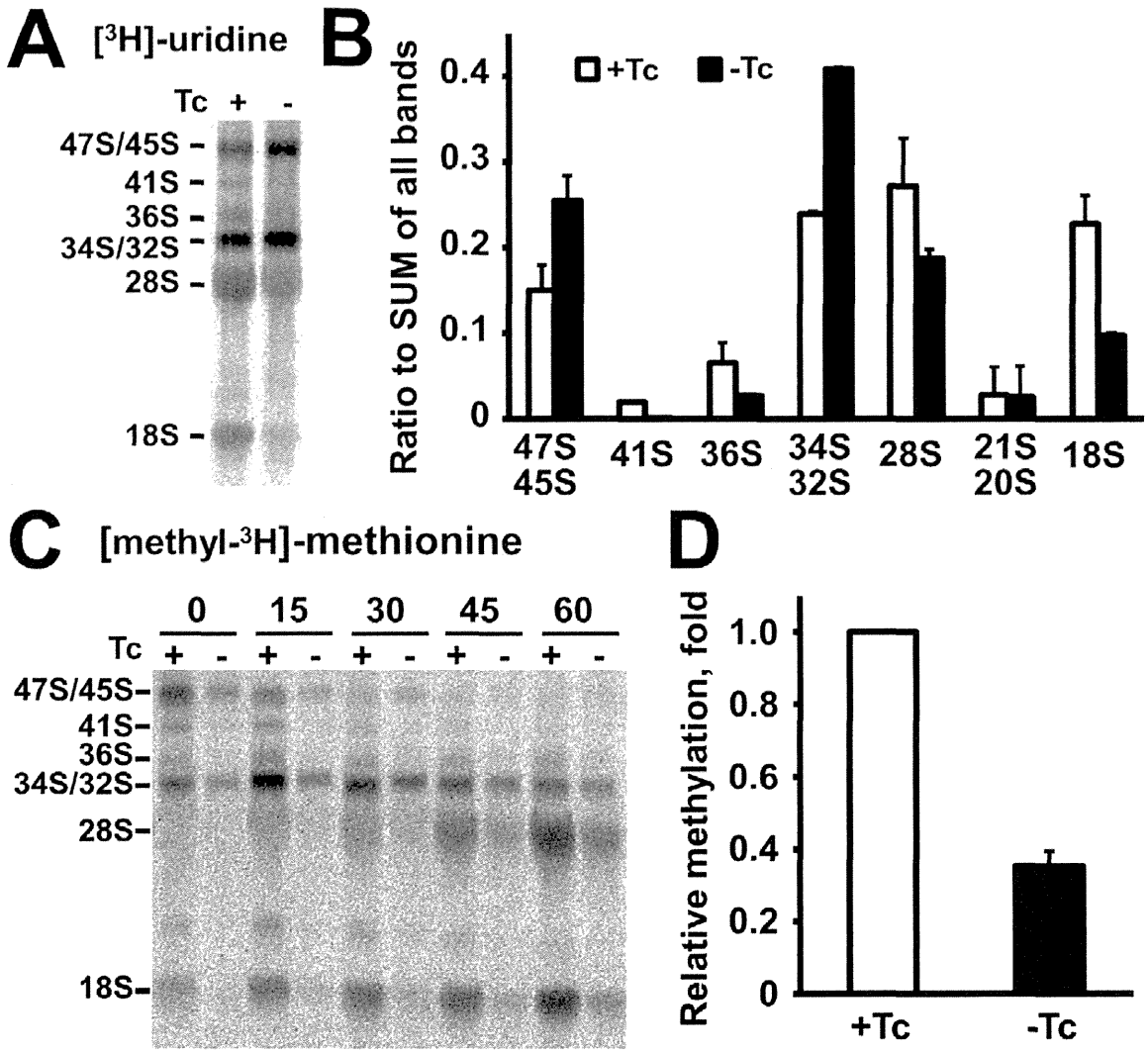

Figure 5. p53 signaling was specifically activated in FBL-knockdown ES cells. (A) Pathway analysis of microarray data obtained with FBL-knockdown ES cells. ES cells were cultured in the absence of Tc for 2 days. p53 signaling was identified as the most activated canonical pathway after knockdown of FBL. (B) Immunofluorescence analysis of p53 and p53 phosphorylation at Ser18 and Ser389 in FBL-knockdown ES cells cultured in the absence of Tc for 2 days. (C) Western blot analysis of p53 protein in ES cells cultured for 2 days without Tc. The lower graph shows the comparison of relative densitometric values of the bands. Values were normalized to Gapdh. Expression levels of p53 were 7.8-fold up-regulated in the absence of Tc (FBL-knockdown conditions). (D) Co-immunoprecipitation analysis of L11 and Mdm2 interaction using ES cells cultured for 2 days after knockdown of FBL. Scale bar: (B), 20 μm. *$p < 0.01$ in (C).

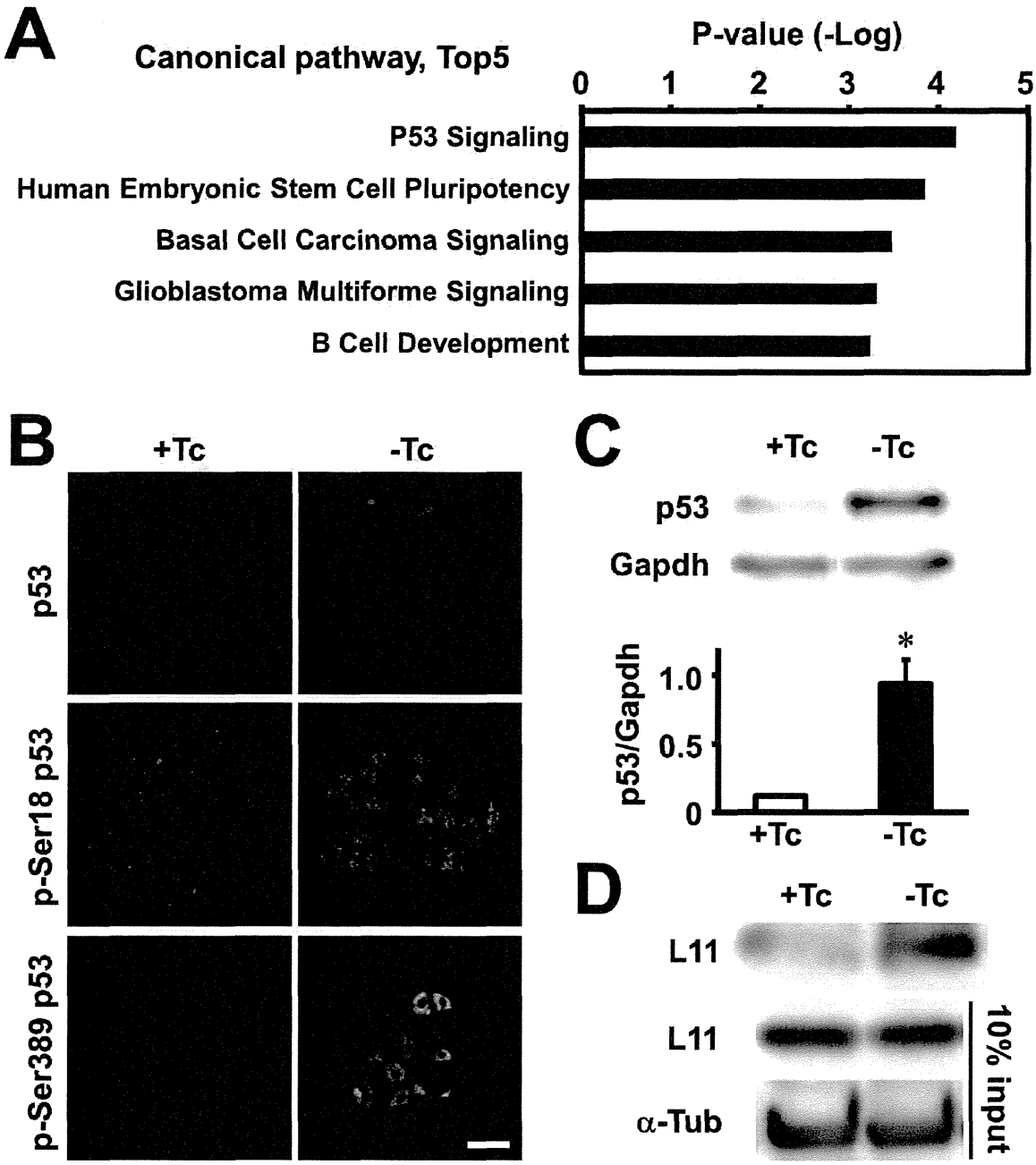

Figure 6. Reduction of FBL expression induces differentiation marker expression via the p53 signaling pathway under self-renewal culture conditions. (A) ES cells cultured for 6 days with 5 ng/mL of Tc resulted in the loss of the densely packed morphology. (B) Immunofluorescence analysis of FBL in (A). (C) Western blot analysis of ES cell extracts after partial knockdown of FBL. FBL expression was decreased to about one-third of that of control conditions after 6 days of culture with 5 ng/mL Tc. (D) qRT-PCR analysis of differentiation- and pluripotency-specific marker expression for each culture condition. After 6 days of culture, the expression of differentiation markers increased, whereas the expression of pluripotency markers was not changed under FBL-reduced conditions. (E) qRT-PCR analysis of differentiation- and pluripotency-specific marker expression 24h after administration of 4 ng/mL actinomycin-D (ActD). (F) Morphological changes in ES cells. ES cells were cultured under self-renewal conditions, and pifithrin-α (PFTα) or DMSO was added from the beginning of culture. In the presence of PFTα, colonies retained their densely packed morphology, even after partial knockdown of FBL. (G) qRT-PCR analysis of the expression of differentiation markers. PFTα treatment suppressed the expression of differentiation markers, *T* and *Fgf5*, in a dose-dependent manner. $*p < 0.01$ in (C, E, and G). $*p < 0.05$ in (D). Scale bars: (A) 300 μm; (B) 10 μm; (F) 500 μm.